UNIVERSITÀ DEGLI STUDI DI PADOVA
DIPARTIMENTO DI TECNICA E GESTIONE DEI SISTEMI INDUSTRIALI

Corso di Laurea Magistrale in Ingegneria Gestionale

Tesi di Laurea Magistrale

The Digital Weldability Test: Predicting Laser Weld Soundness from Input Parameters Using Machine Learning

Relatore: Prof. Paolo Ferro

Correlatore: Prof. Saveria Spiller

Laureando: Muhammad Danish

ANNO ACCADEMICO 2025/2026

Acknowledgement

I would like to express my sincere gratitude to all those who contributed, directly and indirectly, to the successful completion of this master's thesis. First, I would like to extend my deepest appreciation to my supervisor, Professor Paolo Ferro for his continuous academic guidance, valuable feedback, and encouragement throughout all phases of this research. His expertise, patience, and commitment were fundamental in shaping the research framework, methodology, and overall quality of this thesis. I am also sincerely grateful to my co-supervisor, Saveria Spiller for her insightful suggestions, constructive criticism, and professional support during my thesis. Their contributions greatly assisted in refining the research objectives, analytical approach, and interpretation of results applying conceptual modelling using Machine Learning. Furthermore, I would like to acknowledge the faculty members and administrative staff of the University of Padova, particularly those within the Department of Management Engineering, for providing an excellent academic environment, access to learning resources, and continuous support throughout the master's program. The knowledge and skills gained during my studies were essential for the successful completion of this research thesis. I would also like to express my sincere appreciation to all professors and teachers who took part for completing my studies. Their valuable time, practical insights, and willingness to share their experiences significantly contributed to the empirical analysis and the overall findings of this study. In addition, I am thankful to my classmates and colleagues for their cooperation, stimulating discussions, and mutual support during the course of this academic journey. Their encouragement created a positive and motivating learning experience.

Finally, I would like to express my deepest gratitude to my family and friends for their unwavering support, understanding, and motivation throughout my studies. Their patience and confidence in me were a constant source of strength and inspiration.

Abstract

The thesis investigates the weldability and mechanical performance of nickel-based superalloys, using laser beam welding (LBW) techniques and artificial neural network (ANN) modeling. Nickel-based superalloys are widely utilized in high-temperature and corrosive environments such as aerospace, power generation, and chemical industries due to their exceptional mechanical strength, thermal stability, and resistance to oxidation and corrosion. However, their welding presents significant challenges, including crack formation, microstructural instability, and the formation of undesirable intermetallic phases such as Laves phases. The study begins with a comprehensive review of nickel-based alloys, their compositions, and conventional and advanced welding techniques. Particular emphasis is placed on laser beam welding, which offers advantages such as reduced heat input, narrow heat-affected zones, improved weld precision, and minimized distortion compared to traditional methods. The research compiles an extensive database from existing literature, including welding parameters such as laser power, welding speed, alloy composition, and material thickness, alongside corresponding weld quality outcomes. A detailed analysis is conducted to understand the relationship between process parameters and weld quality, including the influence of aluminum and titanium content, laser power, and welding speed on mechanical properties such as tensile strength and hardness. Experimental findings from literature indicate that laser welding can produce high-quality joints with reduced defects, although challenges such as reduced ductility and phase formation persist under certain conditions.

To address the complexity and nonlinearity of welding parameter optimization, an artificial neural network model is developed using MATLAB. The ANN is trained on the compiled dataset to predict weld quality based on input parameters. The model demonstrates strong learning capability, effective convergence behavior, and satisfactory generalization in predicting weld outcomes. Performance evaluation using training results, confusion matrices, and classification metrics confirms the reliability and efficiency of the proposed model. Overall, this research highlights the potential of combining advanced laser welding techniques with data-driven approaches such as ANN to optimize welding parameters and improve the performance of nickel-based superalloy joints. The findings contribute to enhanced process understanding and provide a foundation for intelligent welding system development in advanced manufacturing applications.

Sommario

La tesi indaga la saldabilità e le prestazioni meccaniche delle superleghe a base di nichel, utilizzando tecniche di saldatura laser (LBW) e modellazione con reti neurali artificiali (ANN). Le superleghe a base di nichel sono ampiamente utilizzate in ambienti ad alta temperatura e corrosivi, come quelli aerospaziali, della produzione di energia e dell'industria chimica, grazie alla loro eccezionale resistenza meccanica, stabilità termica e resistenza all'ossidazione e alla corrosione. Tuttavia, la loro saldatura presenta sfide significative, tra cui la formazione di cricche, l'instabilità microstrutturale e la formazione di fasi intermetalliche indesiderate come le fasi di Laves. Lo studio inizia con una revisione completa delle leghe a base di nichel, delle loro composizioni e delle tecniche di saldatura convenzionali e avanzate. Particolare enfasi è posta sulla saldatura laser, che offre vantaggi quali un ridotto apporto di calore, zone termicamente alterate ristrette, una maggiore precisione di saldatura e una distorsione minimizzata rispetto ai metodi tradizionali. La ricerca compila un ampio database dalla letteratura esistente, includendo parametri di saldatura come potenza del laser, velocità di saldatura, composizione della lega e spessore del materiale, insieme ai corrispondenti risultati di qualità della saldatura. È stata condotta un'analisi dettagliata per comprendere la relazione tra i parametri di processo e la qualità della saldatura, inclusa l'influenza del contenuto di alluminio e titanio, della potenza del laser e della velocità di saldatura sulle proprietà meccaniche come la resistenza alla trazione e la durezza. I risultati sperimentali presenti in letteratura indicano che la saldatura laser può produrre giunti di alta qualità con difetti ridotti, sebbene permangano problematiche quali la ridotta duttilità e la formazione di fasi in determinate condizioni.

Per affrontare la complessità e la non linearità dell'ottimizzazione dei parametri di saldatura, è stato sviluppato un modello di rete neurale artificiale (ANN) utilizzando MATLAB. L'ANN è stata addestrata sul dataset compilato per prevedere la qualità della saldatura in base ai parametri di input. Il modello dimostra una forte capacità di apprendimento, un comportamento di convergenza efficace e una soddisfacente generalizzazione nella previsione dei risultati di saldatura. La valutazione delle prestazioni tramite i risultati dell'addestramento, le matrici di confusione e le metriche di classificazione conferma l'affidabilità e l'efficienza del modello proposto. Nel complesso, questa ricerca evidenzia il potenziale della combinazione di tecniche avanzate di saldatura laser con approcci basati sui dati, come le ANN, per ottimizzare i parametri di saldatura e migliorare le prestazioni dei giunti di superleghe a base di nichel. I risultati contribuiscono a una migliore comprensione del processo e forniscono una base per lo sviluppo di sistemi di saldatura intelligenti in applicazioni di produzione avanzata.

Table of Contents

CHAPTER 1 1
INTRODUCTION 1
Superalloys 1
Nickel-based alloys and their compositions 1
Welding and its techniques 4
Artificial Neural Network 6
Goals 7
CHAPTER 2 9
EXAMPLE OF INVESTIGATION ON LASER WELDING OF NICKEL-BASED ALLOY 9
CHAPTER 3 13
METHODOLOGY 13
Creation of Data Base 13
Investigation of Nickel-Based Alloys 26
Welding results 26
Relation between Laser Power and Welding Speed 27
Relation between Aluminum and Titanium on weld quality 28
Neural Network Modelling 31
Neural Network Implementation on MATLAB 32
CHAPTER 4 35
RESULTS 35
Analysis of classification performance and confusion matrix 36
Training results and convergence patterns 37
Model effectiveness and generalization capabilities 38
Final assessment of neural network efficacy 39
CHAPTER 5 41
CONCLUSIONS 41
Overview of the Research 41
1. Key Findings from Literature Review and Database Construction 41
2. Effect of Laser Power and Welding Speed on Weld Quality 42
3. Evaluation of the Al-Ti Weldability Criterion 42
4. Performance of the Artificial Neural Network Model 43
5. Classification Accuracy and Confusion Matrix Analysis 43

6. Training Convergence and Generalization Behavior 44
Contributions of the Research 45
Limitations of the Study 45
Recommendations for Future Work 46
Final Remarks 47
REFERENCES 49

List of Figures

Figure 1. Materials used in Rolls-Royce's Engine *(Akca & Gürsel, 2015)*.. 3

Figure 2. Different shapes and sizes of weld cross-sections obtained through various welding techniques(Donnini et al., 2025).. 5

Figure 3. Neural Network *(Cburnett, 2006)*.. 7

Figure 4. Hardness tests of the Inconel 718 (Thejasree et al., 2022a)..10

Figure 5. Stress vs Strain Curve from tensile experiments of IN718 (Thejasree et al., 2022a).....................10

Figure 6. Bar Graph showing the distribution of the Nickel-Based alloys included in the data base.......... 26

Figure 7. Results of Laser-Beam welding of Nickel-Based Alloys.. 27

Figure 8. Dispersion Graph shows the relation between Laser Power (KW) and welding speed (mm/s) on weld quality 28

Figure 9. shows the Al-Ti compositions of different alloys and its weld quality... 30

Figure 10. Confusion matrix showing classification performance of the neural network on the test dataset 35

Figure 11. Cross-Entropy performance of the neural network during training 38

List of Tables

Table 1. Nickel-Based alloys and their compositions (Sorell, 1997) ………………………………………………………. 3

Table 2. Composition of IN718 in wt% (Thejasree et al., 2022a) ……………………………………………………………. 9

Table 3. Welding parameters of the Laser Beam (Thejasree et al., 2022a)……………………………………………. 9

Table 4. Database ………. 25

Nomenclature

Symbol / Abbreviation	Full Name	Description / Unit
°C	Degrees Celsius	Unit of temperature used throughout the thesis
AISI	American Iron and Steel Institute	A standards organisation whose designations are used to classify steel and alloy grades
Al	Aluminium	Alloying element in nickel-based superalloys that promotes γ′ precipitation hardening
ANN	Artificial Neural Network	A computational model inspired by biological neural networks, used to predict weld quality from input parameters
ATI	Allegheny Technologies Incorporated	Materials manufacturer; ATI 718Plus is a higher-temperature variant of IN718
CE	Cross-Entropy	Loss function used during ANN training to evaluate classification performance
Co	Cobalt	Alloying element used in superalloys to improve high-temperature strength
Cr	Chromium	Alloying element providing oxidation and corrosion resistance
EBW	Electron Beam Welding	A fusion welding process that uses a high-velocity electron beam in a vacuum environment
Fe	Iron	Secondary base element present in several nickel-based superalloy grades
FZ	Fusion Zone	The region of base metal that melts and re-solidifies during welding
GPa	Gigapascal	Unit of elastic modulus (1 GPa = 1000 MPa)

Symbol / Abbreviation	Full Name	Description / Unit
GTAW	Gas Tungsten Arc Welding	An arc welding process that uses a non-consumable tungsten electrode; also known as TIG welding
HAZ	Heat-Affected Zone	The region of base material whose microstructure and properties have been altered by welding heat without melting
Hf	Hafnium	Minor alloying element improving oxidation resistance and grain boundary strength
HI	Heat Input	Energy per unit length delivered to the workpiece during welding; influences HAZ size and microstructure
HV	Vickers Hardness	A hardness measurement obtained using a pyramidal diamond indenter; dimensionless (HV)
IN718	Inconel 718	A precipitation-hardened nickel-based superalloy widely used in aerospace and high-temperature applications
kW	Kilowatt	Unit of laser power (1 kW = 1000 W)
Laves Phase	Intermetallic Compound (AB_2)	Brittle intermetallic compound that forms during solidification of IN718 welds, depleting strengthening elements
LBW	Laser Beam Welding	A high-energy welding process that uses a focused laser beam to join materials with narrow heat input
MATLAB	Matrix Laboratory	A numerical computing environment used for ANN model development and simulation in this thesis
mm/s	Millimetres per Second	Unit of welding speed
Mo	Molybdenum	Solid-solution strengthening element in nickel-based superalloys

Symbol / Abbreviation	Full Name	Description / Unit
MPa	Megapascal	Unit of stress and pressure (1 MPa = 1 N/mm^2)
MSE	Mean Squared Error	Performance metric measuring the average squared difference between predicted and actual values
Nb	Niobium	Key alloying element in IN718; promotes δ-phase and reduces hot cracking susceptibility
Nd:YAG	Neodymium-doped Yttrium Aluminium Garnet	A solid-state laser medium commonly used in pulsed laser welding processes
Ni	Nickel	Primary base element of nickel-based superalloys
P	Laser Power	Energy output of the laser source; measured in kilowatts (kW)
Re	Rhenium	Refractory element added to advanced single-crystal alloys to enhance creep performance
Ru	Ruthenium	Platinum group element used in 5th-generation single-crystal superalloys
SEM	Scanning Electron Microscopy	An imaging technique used to analyse fracture surfaces and microstructural features of weld specimens
Si	Silicon	Minor alloying element improving oxidation and nitriding resistance
t	Material Thickness	Thickness of the workpiece being welded; measured in millimetres (mm)
Ta	Tantalum	Refractory element added to single-crystal superalloys for improved creep resistance
Ti	Titanium	Alloying element contributing to age hardening; used alongside Al to assess weldability

Symbol / Abbreviation	Full Name	Description / Unit
UTS	Ultimate Tensile Strength	Maximum stress a material can withstand before fracture; measured in MPa
v	Welding Speed	Traverse speed of the laser beam along the weld line; measured in mm/s
W	Tungsten	Solid-solution strengthening element used in high-temperature alloys
WEDM	Wire Electrical Discharge Machining	A manufacturing process used to cut specimens for mechanical testing
wt%	Weight Percentage	Unit expressing the proportion of an element in an alloy by mass
γ (gamma)	Austenitic Matrix Phase	Face-centred cubic (FCC) solid-solution matrix phase of nickel-based superalloys
γ′ (gamma prime)	Precipitate Strengthening Phase	Ordered intermetallic phase (Ni_3Al/Ti) responsible for precipitation hardening in nickel superalloys

CHAPTER 1

INTRODUCTION

Superalloys

Superalloys are very important materials that are widely used because they have excellent strength and are highly corrosion-resistant. These qualities make them a top choice for various engineering applications, including those in the aerospace industry, such as aircraft. Superalloys are alloys that contain a high amount of nickel, cobalt or iron and they are grouped into these three types, Nickel-based, Cobalt-based, and Iron-based superalloys, based on the main metal. They keep their structure, surface, and properties stable even at very high temperatures, under heavy stress, and in harsh conditions. This definition covers all current superalloys and allows for new materials to be included. They combine strong mechanical properties with resistance to surface damage. These alloys are mainly used in coal conversion plants, chemical processing, and other areas where heat or corrosion resistance is needed. Their most common use is in making gas turbines for aircraft, power plants, and ships. Superalloys are also important in the oil and gas industry, space vehicles, submarines, nuclear reactors, military motors, chemical processing equipment, and heat exchanger tubes. (Akca & Gürsel, 2015), but the main topic of this thesis is Nickel-based superalloy. In addition, due to their high melting temperature, they often undergo heat treatments to improve their properties, as in the fabrication of trays, baskets, and fittings, as well as heat exchangers in the petroleum processing sector.

Nickel-based alloys and their compositions

Nickel-based alloys demonstrate better resistance to heat and corrosion, which makes the material ideal to be used in higher temperature applications ranging from -150 °C to 1400 °C. They play an extremely important role in hot conditions. Nickel-based alloys are also used in reciprocating engines, metal processing, medical, surgical, and pollution control equipment such as scrubbers. Because of the usage of nickel-based alloys in very severe environments, they are among the most challenging superalloys to machine in order to meet production and quality requirements. They have exceptional strength and resistance to oxidation at temperatures above 550°C, thus making up 45–50% of the total material needed to manufacture an aircraft engine. Wrought (bar, sheet, massive forgings) and casting processes are used to create nickel-based alloys (E.O. Ezugwu et al., 1999).

According to Akca and Gursel, (Akca & Gürsel, 2015) below are some of the nickel-based superalloys with their composition and uses:

- Inconel Alloy 600 (76%Ni, 15% Cr, 8% Fe) is a standard material of construction for nuclear reactors, also used in the chemical industry in heaters, stills, evaporator tubes and condensers.
- Nimonic alloy 75 (80/20 nickel-chromium alloy with additions of titanium and carbon) used in gas turbine engineering, furnace components and heat-treatment equipment.
- Alloy 601 has lower nickel (61%) content with aluminum and silicon additions for improved oxidation and nitriding resistance chemical processing, pollution control, aerospace, and power generation.
- Alloy X750 adds aluminium and titanium for age hardening. Used in gas turbines, rocket engines, nuclear reactors, pressure vessels, tooling, and aircraft structures.
- Alloy 718 (55%Ni, 21%Cr, 5%Nb, 3%Mo), Niobium addition to overcome cracking problems during welding. Used in aircraft, land-based gas turbine engines and cryogenic tankage. Precipitation-hardened superalloy i.e. Inconel 718 has exceptional properties like corrosion resistance, toughness, and stress-rupture resistance. These are carried out at very high temperature upto 1500 °C (Qian & Lippold, n.d.) This material is widely utilized in a variety of industrial components, that includes rocket components and aero-engine hot sections. Despite its unique features, the high cost of production prevented its widespread use. (Liu et al., 2017).
- Alloy X (48%Ni, 22%Cr, 18%Fe, 9%Mo, W). High-temperature flat-rolled product for aerospace applications.
- Waspaloy (60%Ni, 19%Cr, 4%Mo, 3%Ti, 1.3%Al) is used as primary alloy for jet engine applications.
- ATI 718Plus, it's a lower-cost alloy that exceeds the operating temperature capability of standard 718 alloy by 100°F (55°C) allowing engine manufacturers to improve fuel efficiency.
- Nimonic 90 (Ni 54% min, Cr 18-21%, Co 15-21%, Ti 2-3%, Al 1-2%) used for turbine blades, discs, forgings, ring sections and hot-working tools.
- Rene N6 (4%Cr, 12%Co, 1%Mo, 6%W, 7%Ta, 5.8%Al, 0.2% Hf, 5% Re, Bal.Ni) 3rd generation single crystal alloy used in jet engines.
- TMS 162 (3%Cr, 6%Co, 4%Mo, 6%W, 6%Ta, 6%Al, 5%Re, 6%Ru, balance Ni) 5th generation single crystal alloy for turbine blades (Akca & Gürsel, 2015)

Table 1 shows some other corrosion-resistant Nickel-Based Alloys with their composition in wt%: (Sorell, 1997)

Table Nominal composition of corrosion-resistant nickel alloys (wt %).

Alloy	UNS no.	Ni	Cr	Mo	Fe	W	Cu	Other
200	N02200	99.6						
400	N04400	66.5			1.0		31.5	1.0 Mn
600	N06600	75.0	15.5		8.0			
625	N06625	62.0	21.5	9.0	2.5			3.8(Nb+Ta)
690	N06690	61.0	29.0		9.0			
825	N08825	42.0	21.5	3.0	29.5		2.3	1.0 Ti
G-3	N06985	44.0	22.0	7.0	19.5	1.5*	2.0*	2.1 Nb
G-30	N06030	43.0	29.8	5.0	15.0	2.8	1.7	1.0(Nb+Ta)
C-276	N10276	57.0	15.5	16.0	5.5	3.8		
C-22	N06022	56.0	22.0	13.0	3.0	3.0		
C-2000	N10200	59.0	23.0	16.0	1.5		1.6	
622	N06022	58.0	20.5	14.2	2.3	3.2		
686	N06686	60.0	21.0	16.0	5.0*	3.7		
59	N06059	60.0	23.0	15.8	1.5*			
B-2	N10665	69.0	1.0*	28.0	2.0*			
B-3	N10675	68.5	1.5	28.5	1.5	3.0*		
B-4	N10629	66.0	1.0	28.0	3.5			

*Maximum

Table 2. Nickel-Based alloys and their compositions (Sorell, 1997)

Figure 1 below, illustrates Nickel and other materials that are used in the manufacturing of Rolls-Royce aerospace engines: (Akca & Gürsel, 2015)

Table 3

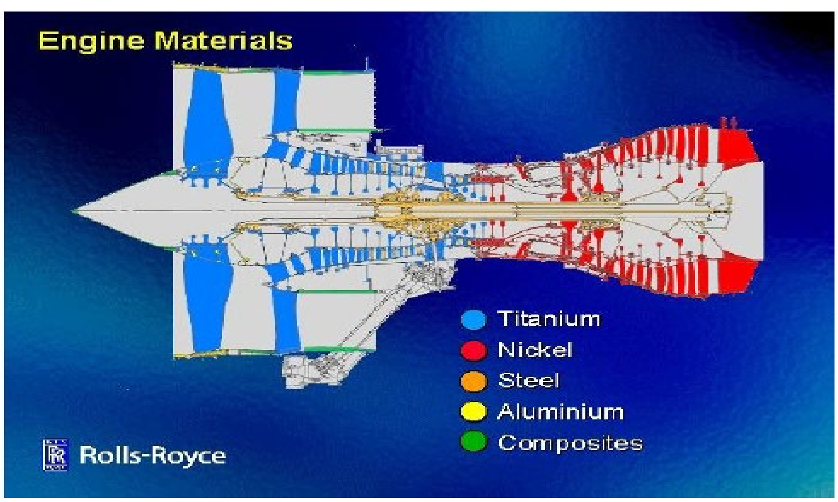

Figure 1. Materials used in Rolls-Royce's Engine (Akca & Gürsel, 2015)

Nickel-based alloys have fully austenitic microstructures because most of the grades used in the chemical industry are solid-solution strengthened, gaining extra strength from elements like molybdenum and tungsten instead of carbide formation. Like austenitic stainless steels, these alloys can only be strengthened by cold working, not by heat treatment. There is another group of nickel-based alloys that are strengthened by precipitation hardening heat treatment. These are mainly used for ultrahigh-strength needs, such as deep oil and gas production or very high-pressure processes. In chemical plants, precipitation-hardened nickel alloys are mostly limited to certain valve and rotating machinery parts. They are more commonly used as heat-resistant superalloys in various applications (Sorell, 1997)

Welding and its techniques

Welding is the process that is used to join metals with the help of high heat input. In the fabrication and repairing of Ni-based superalloy parts like turbine blades, vanes, and casings, gas tungsten arc welding (GTAW) is often used. A typical turbine-blade repair involves removing the damaged leading edge and welding on a patch, which is then shaped to match the original. This process can be costly and uses a lot of material. Also, GTAW repairs are subject to cracking because of the high heat input that causes large shrinkage stresses. High-energy welding methods like laser beam welding (LBW) and electron beam welding (EBW) can help to avoid some of these problems. They improve weldability and reduce the risk of cracking in the heat affected zone (HAZ) by using less heat, which also affects the microstructure and mechanical properties. Specifically:

• Reduced heat input results in narrower seams with decreased Fused Zone (FZ) and Heat-Affected Zone (HAZ).
• A fast-cooling rate minimized grain growth in the heat-affected zone and segregation.
• Restricted development of harmful formations.
• Improved heat distribution resulting in reduced residual stresses.

Indeed, both Electron beam and Laser beam possess significant power, yet they deliver highly concentrated heat input, which confines the amount of material that melts and decreases the total heat exposure that the joints experience. This offers various advantages as explained in the previously mentioned points. Figure2 below illustrates the various shapes and sizes of typical weld cross-sections achieved through different techniques, emphasizing that EBW and LBW generate very narrow beams. (Donnini et al., 2025). In many research works, the impact of LBW on the structural characteristics of the connected components was examined. The results of the research showed that the intensity and velocity of the laser beam influenced the cross-sectional shapes of the interconnected parts. (Ahmad et al., 2021a; Dipali Pandya & Nilesh Ghetia, 2020; Pasupuleti Thejasree & P. C. Krishnamachary, 2022)

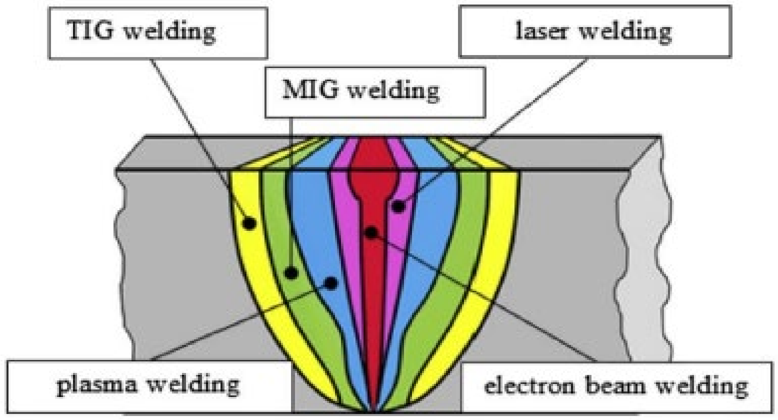

Figure 2. Different shapes and sizes of weld cross-sections obtained through various welding techniques(Donnini et al., 2025)

Although the operational expenses are considerable, Laser beam techniques are well-suited for use in industrial settings as their speed and precision contribute to increased productivity, making them ideal for incorporation into automated manufacturing lines. Additionally, they provide design versatility, and welding can be performed with or without the addition of filler materials, which is called autogenous welding, which lowers the costs of consumable items. (Donnini et al., 2025). Unlike traditional welding techniques, the high-energy beam welding induces a small heat affected zone (HAZ), deep penetration, and rapid processing to create superior welds between diverse materials such as steel and nickel-based superalloy. This method is perfect for creating strong and efficient welds between different metals, including Inconel 718, which is a key material utilized in various fields. Although a variety of literature exists on the welding of nickel-based alloys with different joining methods, welding of thin sheets like up to 1 mm remains difficult, yet it has broader applications in the production of various components (Khan et al., 2012).

Hence, research has been performed to examine the mechanical characteristics of laser welded Inconel 718 alloy thin plates, the tensile strength and hardness of the welded joints have been examined and assessed for enhanced weldments. For example, in the study by Thesarjee, the weldments exhibit robust mechanical properties, including tensile strength and hardness (Thejasree et al., 2022a). Researchers are currently examining the different characteristics of various weldments to determine which methods can prevent the formation of Laves because these are intermetallic compounds that exhibit a stoichiometry of AB2 and are created when the atomic size ratio lies between 1.05 and 1.67. Three types of Laves phases exist: Cubic MgCu2 (C15), Hexagonal MgZn2 (C14), and Hexagonal MgNi2 (C36). They are fragile intermetallic compounds that create issues such as embrittlement, decreased ductility/toughness, sites for crack initiation, and the depletion of strengthening elements (such as Nb) from the matrix, resulting in inferior mechanical performance, particularly at low temperatures or during welding (Rogl & Chen, 2013). To prevent the formation of Laves phases in Inc718, it is possible to use the Laser Beam Welding method, and by incorporating materials with reduced niobium content, since a quick cooling rate and steep temperature gradients can significantly influence the creation of the intermetallic compound. In this way, the weldment's performance can be significantly improved in comparison to the usual joining method. (Devendranath Ramkumar et al., 2018; Lee et al., 2003; Yoshiki Oshida & Toshihiko Tominaga, 2020). While LBW of Inconel 718 joints enhances weld strength, it diminishes malleability because of the rising speed of welding. So, pulsed Nd:YAG welding technique is used, which provides greater control over heat input compared to continuous laser welding. The duration of the pulse, the focused area of the laser, and the frequency of the laser are all factors that affect the quality of a weld in laser welding (Aghayar et al., 2021a; Vemanaboina et al., 2021a). The study found that when the heat input is high, the weld zone on the upper surface is almost the same as that on the lower surface. When the heat input is low, the weld beads, however, are smaller at the bottom (Thejasree, Binoj, et al., 2020) .

Artificial Neural Network

During the production of components with laser welding, selecting and predicting welding parameters is essential to ensure weld quality. Artificial neural networks (ANN), which provide nonlinear mapping between inputs and outputs, offer an alternative approach for developing welding parameter forecasting models. Currently, numerous welding experiments are often required to analyze how welding parameters affect the quality of the weld and to establish standard parameters. This approach consumes significant resources and often yields imprecise results due to experimental limitations. Artificial neural networks (ANN) offer a powerful alternative, as they can learn and approximate nonlinear functions. As a result, ANNs are widely used to identify key factors influencing system characteristics in research. (Yuguang et al., 2013) . An interconnected collection of artificial neurons makes up a neural network, which is a crucial and practical tool for creating models that represent the relationships between both input and output data. Because it can hold a wide collection of parameters, ANN has several advantages in engineering design and group technology. Neural networks are often adaptive systems that change their structure throughout a learning phase. The learning stage of a neural network is important. Neural networks are essential for finding patterns in data or modelling complicated interactions between inputs and outputs. These are simple mathematical models that define a function, distribution, or both. Figure 3 shows the simple Neural Network model (Kumar et al., 2013)

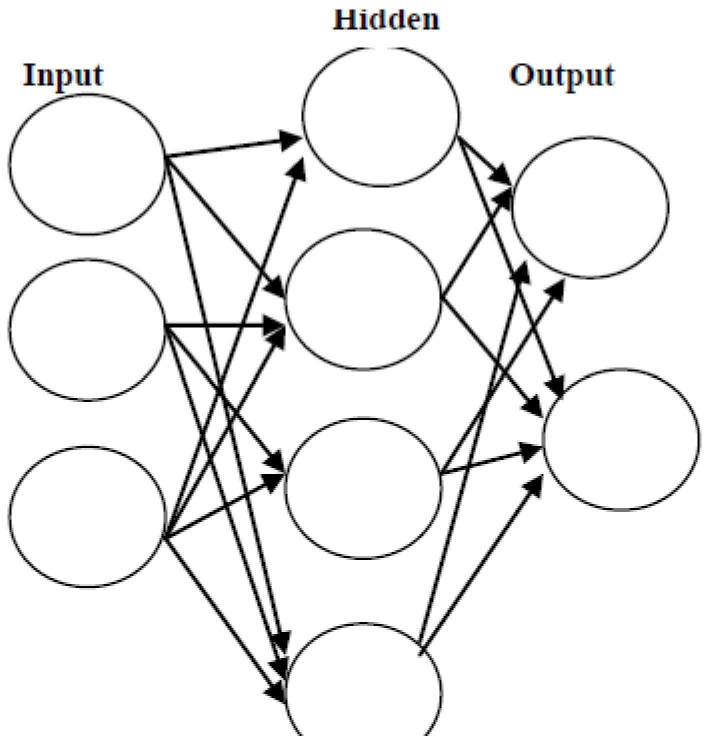

Figure 3. Neural Network (Cburnett, 2006)

Goals

The scope and aim of the thesis are grouped into two sections:

- The first section focuses on developing a database that contains a comprehensive collection of entries related to laser-beam-welded Ni-based alloys, gathering data from literature sources. Specifically, this will include information on chemical compositions, laser welding parameters, and a final evaluation of the weld quality achieved.
- The subsequent section of the thesis will involve utilizing MATLAB software to create a neural network, training it to analyze the previously established database and predict the weldability of the alloys.

CHAPTER 2

EXAMPLE OF INVESTIGATION ON LASER WELDING OF NICKEL-BASED ALLOY

Let's consider an example from the research of (Thejasree et al., 2022a) about the Laser Beam welding of the Nickel-based super alloy Inc718, which is 1 mm in thickness, with the chemical composition shown in Table 2. This alloy has been chosen since it is widely used in industrial applications as discussed above.

	Ni	Cr	Mo	Nb	Co	Cu	Mn	Si	Al	Ti	S	C	Fe
Inc718	50–55	17–21	2.8–3.3	4.75–5.5	1	0.3	0.35	0.35	0.2–0.8	0.7–1.15	0.01	0.08	Bal.

Table 2. Composition of IN718 in wt% (Thejasree et al., 2022a)

The welding parameters that were used during the experiment are shown in Table 3. The sample of alloy was cut with a Wire Electric Discharge Machine (WEDM). After that, the surface was finished and cleaned with acetone and alcohol.

S.NO	Parameters	Values
1	Power	4 KW
2	Pulse Duration	8.0 milli seconds
3	Weld Speed	3.50–2.10 mm/s
4	Heat Output	40.1 J
5	Focal Length	100 mm
6	Beam Width	1.2 mm
7	Frequency	8.0 Hz

Table 3. Welding parameters of the Laser Beam (Thejasree et al., 2022a)

The tensile strength and hardness of the welded sample have been analysed as a durability test. Figure 4 shows the various hardness tests on the base metal plate of IN718. The base metal Inconel 718 exhibited the greatest hardness at 308 HV, which decreased to 205 HV in the heat-affected zone (HAZ). The hardness measurement in the fusion zone (FZ) then rises to 226 HV. However, this value remains lower than that of the original metal. Furthermore, the tensile curve for the weld joint with the highest heat input displays an ultimate strength of 755 MPa, as illustrated in Figure 5. A SEM analysis can reveal the type of fracture that may result from various factors, including the existence of secondary cracks and the surface morphology during welding solidification.

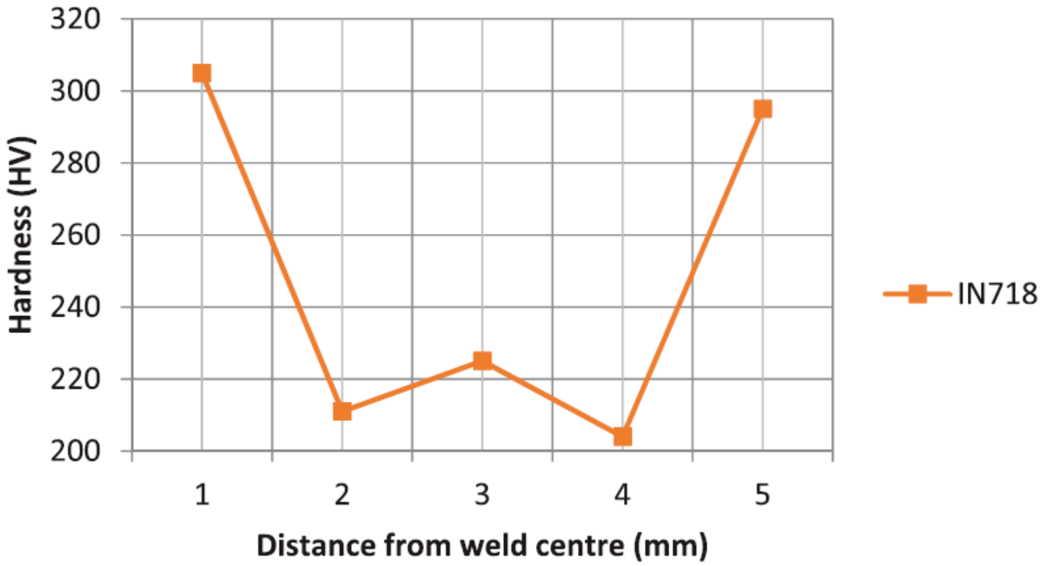

Figure 4. Hardness tests of the Inconel 718 (Thejasree et al., 2022a)

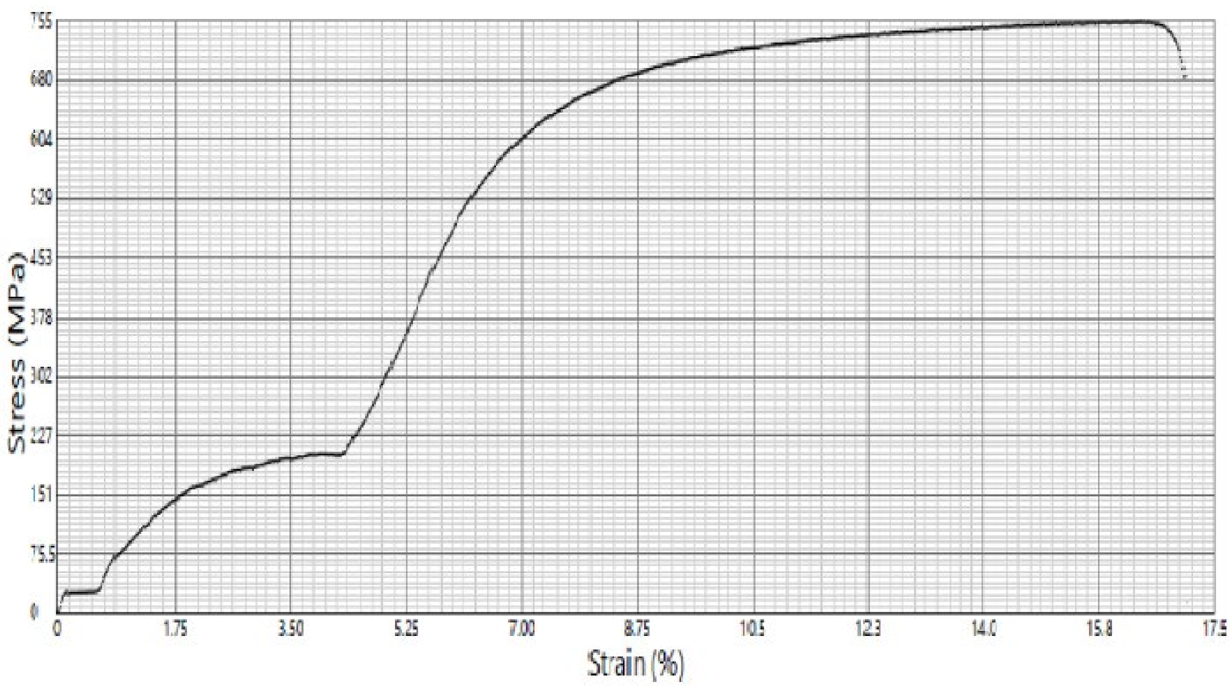

Figure 5. Stress vs Strain Curve from tensile experiments of IN718 (Thejasree et al., 2022a)

The authors concluded that a joint, free of cracks, was achieved through the use of laser welding, highlighting the efficiency of this welding technique. The hardness of the fusion zone (FZ) is lower than that of the base metal, with the variations in grain size between the FZ and the parent metal affecting the hardness. Moreover, the base metal Inconel 718 exhibits the highest hardness at 308 HV. An examination of the tensile strength in the welded joints revealed a clear ductile fracture mode. A fully ductile fracture occurred, generated through the middle of the joint interface (FZ). The research helps us to study the behavior of laser welded joint of Inc718.

CHAPTER 3

METHODOLOGY

Creation of Data Base

In addition to the above-mentioned research paper, there are many other experiments of welding the super alloys with laser beam. Many researchers found that the final joints made by laser beam have good quality with proper penetration, limited cracks and, porosity. However, many results show unacceptable welds. As discussed in the previous chapter, a neural network must be trained to be able to correlate input and output of a problem. To train a neural network, a database shall be constructed. To build a suitable dataset, many research articles were screened to collect the following data: alloy, chemical composition, thickness of the joint, and main laser welding parameters. The summary of all the studies considered, is shown below in Table 4, reporting the alloy name, the main alloying elements, the thickness, the laser power, and the welding speed specifically butt-weds, autogenous, laser welding of Nickel-based alloys.

Nickel-based Alloys	thickness [mm]	laser power [kW]	welding speed [mm/s]	Ni	Al	Ti	Cr	Fe	References
IN625	5	5	25	64.76	0.29	0.38	19.56	1.67	(M. Hong et al., 2022)
IN625	5	5	30	64.76	0.29	0.38	19.56	1.67	
IN625	5	5	35	64.76	0.29	0.38	19.56	1.67	
IN625	0.5	0.26	1.2	67.24	0.099	0.227	20.72	0.319	(Jelokhani-Niaraki et al., 2016)
IN625	0.5	0.23	6	67.24	0.099	0.227	20.72	0.319	
IN718	3.6	3.2	10	54.4	0.6	0.7	17.9	18.65	(Yan et al., 2022)
IN718	1.6	2.90	38.94	54.4	0.6	0.7	17.9	18.65	(OdabaşI et al., 2010)
IN718	1.6	2.512	31.75	54.4	0.6	0.7	17.9	18.65	
IN718	1.6	2	19.89	54.4	0.6	0.7	17.9	18.65	
IN718	1.6	1.5	11.85	54.4	0.6	0.7	17.9	18.65	
IN718	5	6	16.67	54.19	0.49	1.00	17.75	18.2	(J. K. Hong et al., 2008)
IN718	5	6	25.00	54.19	0.49	1.00	17.75	18.2	
IN718	5	6	33.33	54.19	0.49	1.00	17.75	18.2	
IN718	5	6	41.67	54.19	0.49	1.00	17.75	18.2	
IN718	5	6	50.00	54.19	0.49	1.00	17.75	18.2	

IN718	5	6	58.33	54.19	0.49	1.00	17.75	18.2	
IN718	5	6	66.67	54.19	0.49	1.00	17.75	18.2	
IN718	5	5	50.00	54.19	0.49	1.00	17.75	18.2	
IN718	5	5	66.67	54.19	0.49	1.00	17.75	18.2	
IN718	5	7	33.33	54.19	0.49	1.00	17.75	18.2	
IN718	5	7	41.67	54.19	0.49	1.00	17.75	18.2	
IN718	5	7	50.00	54.19	0.49	1.00	17.75	18.2	
IN718	5	7	58.33	54.19	0.49	1.00	17.75	18.2	
IN718	5	7	66.67	54.19	0.49	1.00	17.75	18.2	
IN718	5	8	50.00	54.19	0.49	1.00	17.75	18.2	
IN718	5	8	58.33	54.19	0.49	1.00	17.75	18.2	
IN718	5	8	66.67	54.19	0.49	1.00	17.75	18.2	
IN718	5	10	50.00	54.19	0.49	1.00	17.75	18.2	
IN718	5	10	66.67	54.19	0.49	1.00	17.75	18.2	
IN718	3.2	2.3	33.33	52.2	0.54	1.00	18.4	18.8	(Alvarez et al., 2019)
IN718	3.2	2.3	8.33	52.2	0.54	1.00	18.4	18.8	
IN718	3.2	2.3	33.33	54.6	0.47	0.93	17.7	18.1	
IN718	3.2	2.3	8.33	54.6	0.47	0.93	17.7	18.1	
IN718	3	1.8	23.33	44.22	1.72	0.87	17.8	19.67	(Sharma et al., 2020)
IN718	3	1.8	20.00	44.22	1.72	0.87	17.8	19.67	
IN718	3	1.8	16.67	44.22	1.72	0.87	17.8	19.67	
IN718	2	0.4	2	53	0.51	0.97	17.5	19.75	(Janaki Ram et al., 2005)
Waspaloy	4.3	3	15.83	60.798	1.43	2.87	19.7		(Sekhar & Reed, 2002a)
Udimet 720Li	4.3	3	14.17	57.382	2.46	5.16	15.9		
GH909	2	2	33.33	37.89	0.12	1.66	0.16	40.82	(F. Yan et al., 2017)
GH909	2	3	50	37.89	0.12	1.66	0.16	40.82	
GH909	2	4	66.67	37.89	0.12	1.66	0.16	40.82	
IN625	5	3	16.67	61.87	0.40	0.10	22.00	5.00	(Vemanaboina et al., 2021b)
IN625	5	3	25	61.87	0.40	0.10	22.00	5.00	
IN625	5	3.3	16.67	61.87	0.40	0.10	22.00	5.00	
IN625	5	3.3	25	61.87	0.40	0.10	22.00	5.00	
80A	1.2	1.2	33.33	73.14	1.50	1.60	20.00	2.00	(Saurabh et al., 2024)
80A	1.2	1.2	36.67	73.14	1.50	1.60	20.00	2.00	
80A	1.2	1.2	40	73.14	1.50	1.60	20.00	2.00	
80A	1.2	1.4	33.33	73.14	1.50	1.60	20.00	2.00	
80A	1.2	1.4	36.67	73.14	1.50	1.60	20.00	2.00	

80A	1.2	1.4	40	73.14	1.50	1.60	20.00	2.00	
80A	1.2	1.6	33.33	73.14	1.50	1.60	20.00	2.00	
80A	1.2	1.6	36.67	73.14	1.50	1.60	20.00	2.00	
80A	1.2	1.6	40	73.14	1.50	1.60	20.00	2.00	
IN617	5	4	19	51.72	1.21	0.38	22.82	0.98	(Ren et al., 2015)
IN617	5	5	25	51.72	1.21	0.38	22.82	0.98	
IN617	5	6	42	51.72	1.21	0.38	22.82	0.98	
IN617	5	8	65	51.72	1.21	0.38	22.82	0.98	
IN617	5	6	16.67	51.72	1.21	0.38	22.82	0.98	
IN617	5	8	23.33	51.72	1.21	0.38	22.82	0.98	
IN617	5	10	33.33	51.72	1.21	0.38	22.82	0.98	
IN617	5	12	46.67	51.72	1.21	0.38	22.82	0.98	
Rene 80	1.4	1.6	40	59.59	3	5	15	0.1	(Moradi & Ghoreishi, 2011)
Rene 80	1.4	2.2	40	59.59	3	5	15	0.1	
Rene 80	1.4	1.9	20	59.59	3	5	15	0.1	
Rene 80	1.4	1.9	50	59.59	3	5	15	0.1	
Rene 80	1.4	1	50	59.59	3	5	15	0.1	
Rene 80	1.4	1.9	50	59.59	3	5	15	0.1	
Incoloy 800	4	2	8.33	31	0.15	0.29	20	47.23	(Palanivel et al., 2021)
Incoloy 800	4	2	25.00	31	0.15	0.29	20	47.23	
Incoloy 800	4	2	33.33	31	0.15	0.29	20	47.23	
Incoloy 800	4	2	41.67	31	0.15	0.29	20	47.23	
Haynes 282	5	2	25	57	1.5	2.1	20	1.5	(Osoba et al., 2012)
GH909	2	1.5	25	37.89	0.12	1.66	0.16	40.82	(Zhu et al., 2020)
K418	5	3	15	72	5.95	0.75	12.5	1	(Pang et al., 2008)
Hestalloy X	2	0.075	4	49.32			21.4	17.7	(Pakniat et al., 2016)
Hestalloy X	2	0.3	4	49.32			21.4	17.7	
Hestalloy X	2	0.15	4	49.32			21.4	17.7	
Hestalloy X	2	0.187	4	49.32			21.4	17.7	
Hestalloy X	2	0.225	4	49.32			21.4	17.7	

Hestalloy X	2	0.262	4	49.32			21.4	17.7	
Hestalloy X	2	0.3	10.7	49.32			21.4	17.7	
Hestalloy X	2	0.3	5	49.32			21.4	17.7	
Hestalloy X	2	0.5	10.7	49.32			21.4	17.7	
Hestalloy X	2	0.5	5	49.32			21.4	17.7	
IN738LC	5	0.24	8	59.13	4.36	3.15	15.5	0.09	(Montazeri & Ghaini, 2012)
GH3535	4	1.8	13.33	70.13	0.175	0.175	7.07	4.02	(Jiang et al., 2016)
GH3535	4	2	13.33	70.13	0.175	0.175	7.07	4.02	
GH3535	4	2.2	16.67	70.13	0.175	0.175	7.07	4.02	
GH3535	4	2.4	20	70.13	0.175	0.175	7.07	4.02	
GH3535	4	1.62	13.33	70.13	0.175	0.175	7.07	4.02	
IN792 E	3	1.5	25	59.01	3.05	3.96	12.13		Internal report
IN792 E	3	1.7	25	59.01	3.05	3.96	12.13		
IN792 E	3	1.7	25	59.01	3.05	3.96	12.13		
IN792 E	3	1.5	17	59.01	3.05	3.96	12.13		
IN792 E	3	0.9	8	59.01	3.05	3.96	12.13		
IN792 E	3	0.7	8	59.01	3.05	3.96	12.13		
IN792 E	2	1.25	25.00	59.01	3.05	3.96	12.13		
IN792 E	2	1.25	25.00	59.01	3.05	3.96	12.13		
IN792 E	2	0.56	10.00	59.01	3.05	3.96	12.13		
IN792 E	3	1	10.00	59.01	3.05	3.96	12.13		
IN792 E	3	1	10.00	59.01	3.05	3.96	12.13		
IN718	3	2.2	20	54.44	0.46	0.94		17.62	
IN625 pieno	2.5	1.7	15.00	60.4	0.2	0.2	21.8	3.6	
IN625 pieno	2.5	1.7	20.00	60.4	0.2	0.2	21.8	3.6	
IN625 pieno	2.5	1.7	25	60.4	0.2	0.2	21.8	3.6	
IN625 pieno	2.5	2	15.00	60.4	0.2	0.2	21.8	3.6	
IN625 pieno	2.5	2	20.00	60.4	0.2	0.2	21.8	3.6	
IN625 pieno	2.5	2	25	60.4	0.2	0.2	21.8	3.6	
IN625 pieno	2.5	2.3	15.00	60.4	0.2	0.2	21.8	3.6	
IN625 pieno	2.5	2.3	20.00	60.4	0.2	0.2	21.8	3.6	

IN625 pieno	2.5	2.3	25	60.4	0.2	0.2	21.8	3.6	
IN625 AM horiz	2.4	1.92	25	60.4	0.2	0.2	21.8	3.6	
IN625 AM horiz	2.4	1.632	20	60.4	0.2	0.2	21.8	3.6	
IN625 AM horiz	2.4	1.92	20	60.4	0.2	0.2	21.8	3.6	
IN625 AM horiz	2.4	1.632	25	60.4	0.2	0.2	21.8	3.6	
IN625 AM vert	2.8	2.24	25	60.4	0.2	0.2	21.8	3.6	
IN625 AM vert	2.8	1.9	20	60.4	0.2	0.2	21.8	3.6	
IN625 AM vert	2.8	2.24	20	60.4	0.2	0.2	21.8	3.6	
IN625 AM vert	2.8	1.9	25	60.4	0.2	0.2	21.8	3.6	
AF955	2.5	1.19	17	57.4	0.43	0.86	21.6	8.836	
AF955	2.5	1.36	17	57.4	0.43	0.86	21.6	8.836	
AF955	2.5	1.53	17	57.4	0.43	0.86	21.6	8.836	
AF955	2.5	1.75	25	57.4	0.43	0.86	21.6	8.836	
AF955	2.5	2	25	57.4	0.43	0.86	21.6	8.836	
AF955	2.5	2.25	25	57.4	0.43	0.86	21.6	8.836	
AF955	2.5	2.31	33	57.4	0.43	0.86	21.6	8.836	
AF955	2.5	2.64	33	57.4	0.43	0.86	21.6	8.836	
AF955	2.5	2.97	33	57.4	0.43	0.86	21.6	8.836	
AF955	2.5	1.19	17	57.4	0.43	0.86	21.6	8.836	
AF955	2.5	1.19	13	57.4	0.43	0.86	21.6	8.836	
AF955	2.5	1.19	15	57.4	0.43	0.86	21.6	8.836	
Ni-28W-6Cr	4	2.5	16.6	61.16			6.1		(Tian, Chen, Wang, Tao, Ye, Ren, et al., 2023)
Ni-28W-6Cr	4	4	16.6	61.16			6.1		
IN738	3	4	8.3	71.54	3.5	3.36	16.09	0.07	(Aina, 2014)
IN738	3	4	25	71.54	3.5	3.36	16.09	0.07	
IN738	3	3	33.3	71.54	3.5	3.36	16.09	0.07	
IN738	3	4	33.3	71.54	3.5	3.36	16.09	0.07	
IN738	3	4	42	71.54	3.5	3.36	16.09	0.07	
IN718	3.25	1.8	10	54.19	0.49	1.00	17.75	18.2	(Patil et al., 2025)
GDT-111	1	0.2	8.3	54.19	0.49	1.00	17.75	18.2	(Chen & Taheri, 2020)
GDT-111	1	0.2	8.3	54.19	0.49	1.00	17.75	18.2	

GDT-111	1	0.2	8.3	54.19	0.49	1.00	17.75	18.2	
GDT-111	1	0.2	8.3	54.19	0.49	1.00	17.75	18.2	
GDT-111	1	0.2	8.3	60.4	3	4.9	14		
C-2000	4	2.4	16.7	53.3	0.49		23	3	(Arulmurugan et al., 2021)
New comp	3.2	1	100	52.7	3	7	19		(Naffakh Moosavy et al., 2014)
New comp	3.2	1	100	52.4	2.4	5.5	19	4.6	
New comp	3.2	1	100	52	1.8	4	19	9.4	
New comp	3.2	1	100	51.8	1.2	2.5	19	13.9	
New comp	3.2	1	100	51.4	0.6	1.1	19	18.6	
New comp	3.2	0.4	40	52.7	3	7	19		
New comp	3.2	0.4	40	52.4	2.4	5.5	19	4.6	
New comp	3.2	0.4	40	52	1.8	4	19	9.4	
New comp	3.2	0.4	40	51.8	1.2	2.5	19	13.9	
New comp	3.2	0.4	40	51.4	0.6	1.1	19	18.6	
IN718	2	2	10	52.61	0.51	1.02	19	18.7	(Huang et al., 2025)
IN718	2	2	12	52.61	0.51	1.02	19	18.7	
IN718	2	2	14	52.61	0.51	1.02	19	18.7	
IN718	2	1	10	52.61	0.51	1.02	19	18.7	
IN718	2	1.5	10	52.61	0.51	1.02	19	18.7	
IN718 PLUS	2	3	10	51.48	1.56	1.18	18.22	9.22	
IN718 PLUS	2	3	12	51.48	1.56	1.18	18.22	9.22	
IN718 PLUS	2	3	14	51.48	1.56	1.18	18.22	9.22	
IN718 PLUS	2	2	10	51.48	1.56	1.18	18.22	9.22	
IN718 PLUS	2	2.5	10	51.48	1.56	1.18	18.22	9.22	
GH3539	3	3	60	65.84		0.14	5.8	0.01	(Tian, Chen, Wang, Tao, Ye, Li, et al., 2023)
GH3539	3	4	60	65.84		0.14	5.8	0.01	
GH3539	3	5	60	65.84		0.14	5.8	0.01	
GH3539	3	6	60	65.84		0.14	5.8	0.01	
GH3539	3	7	60	65.84		0.14	5.8	0.01	

GH3539	3	3	40	65.84		0.14	5.8	0.01	
GH3539	3	3	50	65.84		0.14	5.8	0.01	
GH3539	3	3	60	65.84		0.14	5.8	0.01	
GH3539	3	3	70	65.84		0.14	5.8	0.01	
K439B	2	2.1	25	48.7	2.5	2.51	22.02		(LI et al., 2024)
Haynes 188	2	2	66.7	22			22	3	(Allen et al., 2015)
Haynes 189	2	2	50	22			22	3	
IN718	2	2	66.7	52.5	0.5	0.90	19	18	
IN718	2	2	50	52.5	0.5	0.90	19	18	
IN718	5	5.1	43.3	52.5	0.5	0.90	19	18	
IN600	3	2	25	72			15.5	8	
IN600	3	3	50	72			15.5	8	
WASPALOY	1.5	0.2	1.5	57.023	1.42	3.2	19.5	0.9	(Shoja Razavi, 2016)
GTD-111	1	0.209	8.3	69.016	2.8	3	14		(Norouzian et al., 2023)
IN718	4	0.879	2.4	52.944	0.54	1.07	18.33	18.01	(Gobbp et al., 1996)
IN718	2.6	2.5	60	52.5	0.5	0.9	19	16.80	(Voropaev et al., 2019)
IN718	3.6	3.5	40	52.5	0.5	0.9	19	16.80	
IN718	5.1	3.5	25	52.5	0.5	0.9	19	16.80	
IN718	6.1	3.5	10	52.5	0.5	0.9	19	16.80	
Ni-26W6Cr-GH3539	3	1.5	7	65.84		0.14	5.8	0.01	(Tian et al., 2024)
Ni-26W6Cr-GH3539	3	2.0	15	65.84		0.14	5.8	0.01	
Ni-26W6Cr-GH3539	3	3.0	36	65.84		0.14	5.8	0.01	
Ni-26W6Cr-GH3539	3	4.0	50	65.84		0.14	5.8	0.01	
Ni-26W6Cr-GH3539	3	5.0	65	65.84		0.14	5.8	0.01	
GH3535	4	1.68	13.3	70.6	0.07		6.95	4.06	(Yu et al., 2017)
costum	0.8	0.36	20	52.61	0.55	1.1	18.86	18.23	(Yue et al., 2024)
costum	0.8	0.36	20	52.61	0.55	1.1	18.86	18.23	

costum	0.8	0.36	20	52.61	0.55	1.1	18.86	18.23	
costum	0.8	0.504	20	52.61	0.55	1.1	18.86	18.23	
costum	0.8	0.504	20	52.61	0.55	1.1	18.86	18.23	
costum	0.8	0.672	20	52.61	0.55	1.1	18.86	18.23	
costum	0.8	0.672	20	52.61	0.55	1.1	18.86	18.23	
costum	0.8	0.672	20	52.61	0.55	1.1	18.86	18.23	
GTD-111	1	0.112	8.3	60.086	3.1	4.9	14		(Taheri et al., 2021)
GTD-111	1	0.168	8.3	60.086	3.1	4.9	14		
GTD-111	1	0.224	8.3	60.086	3.1	4.9	14		
GTD-111	1	0.28	8.3	60.086	3.1	4.9	14		
GTD-111	1	0.336	8.3	60.086	3.1	4.9	14		
GH4099	2	3	10	61.33	2.09	1.32	18.56		(Yang . Huiping . Zhou, 2025)
GH4099	2	3	8.3	61.33	2.09	1.32	18.56		
GH4099	2	3	5	61.33	2.09	1.32	18.56		
GH4099	2	2.82	5	61.33	2.09	1.32	18.56		
GH4099	2	2.64	5	61.33	2.09	1.32	18.56		
GH4099	2	2.4	5	61.33	2.09	1.32	18.56		
GH3536	1.2	1	20	48.13	0.25	0.09	21.58	18.45	(Hou. Wang.Yong, 2023)
GH909	2	2.5	41.6	18.03	0.12	1.65		60.53	(Zhang . Yang, 2022)
IN617	3	1.5	10	49.14	1.15	0.6	22	3	(H. L. K. Cheng, 2022)
IN617	3	2	10	49.14	1.15	0.6	22	3	
IN617	3	2.5	10	49.14	1.15	0.6	22	3	
IN617	3	2	25	49.14	1.15	0.6	22	3	
IN617	3	2.5	25	49.14	1.15	0.6	22	3	
IN617	3	3	25	49.14	1.15	0.6	22	3	
IN617	1	0.7	10	49.14	1.15	0.6	22	3	
IN617	1	0.9	10	49.14	1.15	0.6	22	3	
IN625	1	1.6	0.02	65.171	0.37	0.2	20.68	0.9	(Hu et al., 2019)
Invar36	5	5	25	36.53			0.026	62.54	(Li . M Gao . Chen, 2013)
IN625	0.8	0.3	33.3	59.60%		0.19%	22.85%	4.81%	(Roy et al., 2025)
Incoloy 800	4	2	33.3	31%	0.15%	0.29%	20%		(Alswat, 2025)
Incoloy 800	4	2.5	33.3	31%	0.15%	0.29%	20%		

Incoloy 800	4	3	33.3	31%	0.15%	0.29%	20%		
IN718	2	0.72	14.17	52.86	0.348	0.976	18.57	17.37	(Seenivasan, 2025)
IN718	2	0.72	10.83	52.86	0.348	0.976	18.57	17.37	
IN718	2	0.55	14.17	52.86	0.348	0.976	18.57	17.37	
IN718	2	0.55	10.83	52.86	0.348	0.976	18.57	17.37	
IN718	2	0.55	10.83	52.86	0.348	0.976	18.57	17.37	
IN718	2	0.42	14.17	52.86	0.348	0.976	18.57	17.37	
IN718	2	0.55	14.17	52.86	0.348	0.976	18.57	17.37	
IN718	2	0.42	10.83	52.86	0.348	0.976	18.57	17.37	
IN718	2	0.44	12.50	52.86	0.348	0.976	18.57	17.37	
IN718	2	0.69	12.50	52.86	0.348	0.976	18.57	17.37	
IN718	2	0.44	12.50	52.86	0.348	0.976	18.57	17.37	
IN718	2	0.69	12.50	52.86	0.348	0.976	18.57	17.37	
IN718	2	0.56	9.70	52.86	0.348	0.976	18.57	17.37	
IN718	2	0.56	15.30	52.86	0.348	0.976	18.57	17.37	
IN718	2	0.56	12.50	52.86	0.348	0.976	18.57	17.37	
IN718	2	0.56	12.50	52.86	0.348	0.976	18.57	17.37	
IN718	2	0.56	12.50	52.86	0.348	0.976	18.57	17.37	
IN718	2	0.56	12.50	52.86	0.348	0.976	18.57	17.37	
IN718	2	0.56	12.50	52.86	0.348	0.976	18.57	17.37	
IN718	2	0.56	12.50	52.86	0.348	0.976	18.57	17.37	
IN718	2	0.56	12.50	52.86	0.348	0.976	18.57	17.37	
IN718	3	3	70	72.06	0.47	0.47	18.13	4.86	(Hamada et al., 2025)
G27	4.2	2.23	7.33	57.86	1.9	1.88	15.11	15	(Ariaseta et al., 2024)
G27	4.2	2.43	7.33	57.86	1.9	1.88	15.11	15	
G27	4.2	2.23	9.33	57.86	1.9	1.88	15.11	15	
G27	4.2	2.43	9.33	57.86	1.9	1.88	15.11	15	
G27	4.2	2.23	7.33	57.86	1.9	1.88	15.11	15	
G27	4.2	2.43	7.33	57.86	1.9	1.88	15.11	15	
G27	4.2	2.23	9.33	57.86	1.9	1.88	15.11	15	
G27	4.2	2.43	9.33	57.86	1.9	1.88	15.11	15	
G27	4.2	2.23	7.33	57.86	1.9	1.88	15.11	15	
G27	4.2	2.43	7.33	57.86	1.9	1.88	15.11	15	
G27	4.2	2.23	9.33	57.86	1.9	1.88	15.11	15	
G27	4.2	2.43	9.33	57.86	1.9	1.88	15.11	15	
G27	4.2	2.23	7.33	57.86	1.9	1.88	15.11	15	
G27	4.2	2.43	7.33	57.86	1.9	1.88	15.11	15	
G27	4.2	2.23	9.33	57.86	1.9	1.88	15.11	15	

G27	4.2	2.43	9.33	57.86	1.9	1.88	15.11	15	
G27	4.2	2.33	8.33	57.86	1.9	1.88	15.11	15	
G27	4.2	2.33	8.33	57.86	1.9	1.88	15.11	15	
G27	4.2	2.33	8.33	57.86	1.9	1.88	15.11	15	
IN825	2	2.1	10	43.52	0.14	0.57	20.7	28.4	(Jaya Kishore Sunkara, 2024)
IN825	2	1.95	10	43.52	0.14	0.57	20.7	28.4	
IN825	2	1.8	10	43.52	0.14	0.57	20.7	28.4	
IN825	2	1.65	10	43.52	0.14	0.57	20.7	28.4	
IN825	2	1.5	10	43.52	0.14	0.57	20.7	28.4	
INX750	1.2	1.2	1.25	69.151	0.79	2.97	15.73	10.05	(Pariyar et al., 2023)
INX750	1.2	1.2	2.5	69.151	0.79	2.97	15.73	10.05	
INX750	1.2	1.2	5	69.151	0.79	2.97	15.73	10.05	
INX750	1.2	0.8	5	69.151	0.79	2.97	15.73	10.05	
INX750	1.2	0.8	2.5	69.151	0.79	2.97	15.73	10.05	
INX750	1.2	0.8	1.25	69.151	0.79	2.97	15.73	10.05	
INX750	1.2	0.4	1.25	69.151	0.79	2.97	15.73	10.05	
IN718	3	0.3	0.5	52.82	0.495	0.959	18.64	17.41	(Ghaffari & Naffakh-Moosavy, 2022)
GH909	5	4.3	25	38.33		1.73		41.17	(Zhengwu Zhu, 2022)
GTD-111	2	1.9	80	60.5	3	4.9	14		(Taheri et al., 2022)
GH909	2	1.5	25	38.25		1.66		40.88	(Zhang et al., 2021)
GH909	2	2	33	38.25		1.66		40.88	
GH909	2	2.5	42	38.25		1.66		40.88	
GH909	2	3	50	38.25		1.66		40.88	
GH909	2	3.5	58	38.25		1.66		40.88	
IN718	2	1.35	2	52.82	0.49	0.959	18.64	17.41	(Keivanloo et al., 2021)
IN718	2	1.35	2	52.82	0.49	0.959	18.64	17.41	
IN718	2	1.35	2	52.82	0.49	0.959	18.64	17.41	
Haynes 25	2	0.247	6	10			20	3	(Graneix et al., 2017)
Haynes 25	2	0.203	3.4	10			20	3	
Haynes 188	1.2	2.097	68.66	23.9			22.1	2.02	
Haynes 188	1.2	2.353	23.16	23.9			22.1	2.02	

Haynes 188	1.2	1.571	127.5	22			22	3	(Graneix et al., 2014)
Haynes 188	1.2	2.43	52.8	22			22	3	
Hastelloy X	1.2	2.097	68.7	47.29			22.1	18.7	
Hestalloy X	1.2	2.353	23.2	47.29			22.1	18.7	
Hestalloy C-276	1.2	0.045	1.66	58.766			16	5.6	(Ma et al., 2015)
GTD-111	1	0.148	8.3	60.39	3	4.9	14		(Taheri et al., 2019)
GTD-111	1	0.173	8.3	60.39	3	4.9	14		
GTD-111	1	0.195	8.3	60.39	3	4.9	14		
GTD-111	1	0.209	8.3	60.39	3	4.9	14		
GTD-111	1	0.253	8.3	60.39	3	4.9	14		
GTD-111	1	0.153	8.3	60.39	3	4.9	14		
GTD-111	1	0.171	8.3	60.39	3	4.9	14		
GTD-111	1	0.19	8.3	60.39	3	4.9	14		
GTD-111	1	0.238	8.3	60.39	3	4.9	14		
GTD-111	1	0.209	5.6	60.39	3	4.9	14		
GTD-111	1	0.209	6.7	60.39	3	4.9	14		
GTD-111	1	0.209	9.3	60.39	3	4.9	14		
GTD-111	1	0.209	13	60.39	3	4.9	14		
Haynes 282	5	2	16.6	41.035	1.5	2.1	20	1.5	(Osobo . Oja, 2011)
Haynes 282	5	2	33.3	41.035	1.5	2.1	20	1.5	
Haynes 188	1	1.2	100	22			22	3	(Yilbas & Akthar, 2011)
Haynes 188	1.2	2.85	46.5	25.66			18.6	2.23	(Odabaşi et al., 2013)
Haynes 188	1.2	2.85	36.4	25.66			18.6	2.23	
Haynes 188	1.2	2.85	31.1	25.66			18.6	2.23	
Haynes 188	1.2	2.5	36.4	25.66			18.6	2.23	
Haynes 188	1.2	2.5	31.1	25.66			18.6	2.23	
Haynes 188	1.2	2.5	26.4	25.66			18.6	2.23	

Haynes 188	1.2	2	31.1	25.66			18.6	2.23	
Haynes 188	1.2	2	26.4	25.66			18.6	2.23	
Haynes 188	1.2	2	22.2	25.66			18.6	2.23	
Inc718	2.5	2.3	8.33	52.9	0.23	0.66	17.6	20	(García-Sesma et al., 2024)
Inc718 mod 1	2.5	2.3	8.33	55.7	0.62	0.92	17.6	17	
Inc718 mod 2	2.5	2.3	8.33	55.5	0.62	0.93	17.6	16.1	
Inc718	5	2.3	8.33	52.9	0.23	0.66	17.6	20	
Inc718 mod 1	5	2.3	8.33	55.7	0.62	0.92	17.6	17	
Inc718 mod 2	5	2.3	8.33	55.5	0.62	0.93	17.6	16.1	
Inc718	1.2	4	3.5	55	0.8	1.15	21	11.16	(Thejasree et al., 2022b)
Inc718	2	3.3	23.33	58.82	1.5	0.425	18	15	(Prakash et al., 2024)
Inc718	3.2	6	8.33	55.6	0.49	1	18.39	16.1	(Yeni. Kocak, 2006)
Inc625	3.2	6	8.33	60.55	0.19	0.28	21.72	4.53	
Inc718Plus	9	3.5	10	51.65	1.45	0.7	18	10	(Lijun Yang, 2024)
Inc718	3	2.2	17.5	55	0.8	1.15	21	11.43	(Zapirain et al., 2011)
Rene41	3	2.2	17.5	52.44	1.6	3.3	20.1		
Inco625	3	2.2	17.5	58	0.4	0.4	20	5	
Hastelloy C-276	0.5	1.5	13.2	58			16	5.14	(B. Cheng et al., 2024)
Hastelloy 304	2	1.5	13.2	8.02			18.2	72.06	
ERNiCrMo-4	1	1.5	13.2	59.63			16	5.3	
Inc601	3	2.3	14	63	1.7		25	8.68	(Aghayar et al., 2021b)
Inc625	1.1	0.886	41.67	59.6	0.6	0.19	22.85	4.81	(Ahmad et al., 2021b)
Inc625	1.1	1.241	58.33	59.6	0.6	0.19	22.85	4.81	
Inc625	1.1	1.595	75	59.6	0.6	0.19	22.85	4.81	
Inc625	1.1	1.95	91.67	59.6	0.6	0.19	22.85	4.81	
Inc718	2	0.8	8.33	52	0.5	0.9	18	19	(Murua et al., 2024)
Inc718	2	0.8	16.667	52	0.5	0.9	18	19	
Inc625	0.7	0.8	20	57.93	0.4	0.4	21.5	5	

Inc625	0.7	0.8	35	57.93	0.4	0.4	21.5	5	(Caiazzo et al., 2017)
Inc625	0.7	0.8	50	57.93	0.4	0.4	21.5	5	
Inc625	0.7	0.8	65	57.93	0.4	0.4	21.5	5	
Inc625	0.7	1	20	57.93	0.4	0.4	21.5	5	
Inc625	0.7	1	35	57.93	0.4	0.4	21.5	5	
Inc625	0.7	1	50	57.93	0.4	0.4	21.5	5	
Inc625	0.7	1	65	57.93	0.4	0.4	21.5	5	
Inc625	0.7	1.2	20	57.93	0.4	0.4	21.5	5	
Inc625	0.7	1.2	35	57.93	0.4	0.4	21.5	5	
Inc625	0.7	1.2	50	57.93	0.4	0.4	21.5	5	
Inc625	0.7	1.2	65	57.93	0.4	0.4	21.5	5	
Inc625	1.5	0.35	5	59.6		0.19	22.85	4.81	(Iskindar Tili, 2022)
Inc625	1.5	0.35	6.667	59.6		0.19	22.85	4.81	
Inc625	1.5	0.35	8.333	59.6		0.19	22.85	4.81	
Inc625	1.5	0.3	5	59.6		0.19	22.85	4.81	
Inc625	1.5	0.4	5	59.6		0.19	22.85	4.81	
Inc625	1.5	0.075	1.5	61.5	0.4	0.4	20	5	(Thejasree, Manikandan, et al., 2020)
Inc625	1.5	0.1	2	61.5	0.4	0.4	20	5	
Inc625	1.5	0.12	3	61.5	0.4	0.4	20	5	
Inc625	1.5	0.13	4	61.5	0.4	0.4	20	5	
Inc625	1.5	0.15	5	61.5	0.4	0.4	20	5	
Monel400	0.5	0.6	6.667	64.997	0.151	0.008	0.09	2.45	(Shanthos Kumar, 2018)
Monel400	0.5	0.6	6.667	64.997	0.151	0.008	0.09	2.45	
Monel400	0.5	0.6	6.667	64.997	0.151	0.008	0.09	2.45	
Monel400	0.5	0.6	6.667	64.997	0.151	0.008	0.09	2.45	
Monel400	0.5	0.6	6.667	64.997	0.151	0.008	0.09	2.45	
Inc625	1.2	0.18	0.166	61.87	0.40	0.10	22.00	5.00	(Sudhani Srikanth, 2020)
Inc625	1.2	0.19	0.25	61.87	0.40	0.10	22.00	5.00	
Inc625	1.2	0.2	0.333	61.87	0.40	0.10	22.00	5.00	

Table 4. Dataset

Investigation of Nickel-Based Alloys

Figure 6 shows the distribution of the different Nickel-Based alloys that were investigated as reported in the above table. IN718 was the most analyzed alloy, followed by IN625, GTD11, and others. The data was collected from a total of 73 research papers. The label 'Other Nickel-based alloys' include Udimet720Li, K418, GH3535/4099, Ni-28W-6Cr, C-200, K439B, IN600/601, Costum, IN825, Hastelloy C-276/304, Monel400, Invar36, and new alloys.

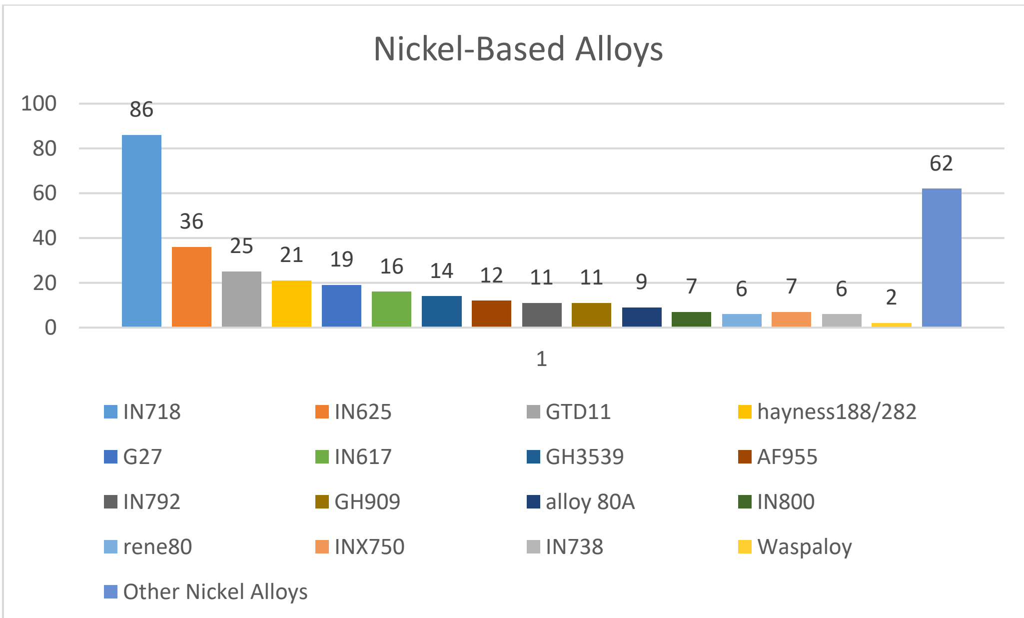

Figure 6. Bar Graph showing the distribution of the Nickel-Based alloys included in the data base.

Welding results

An assessment of the quality of the welds obtained in each of the research articles included in the database is made. After considering different laser parameters, welding speed, thickness of the welds, and alloy composition, the quality of the welds obtained in the research articles of the database is evaluated based on the micrographs and on the observations reported by the authors. The welds are classified into 'good', 'acceptable defects', and 'bad'. The size of each category is shown in Figure 7. There are large numbers of good quality welds achieved, followed by acceptable minor quality defects and undesirable quality. It is to be noted that the same alloy has different results when its composition and laser parameters are changed.

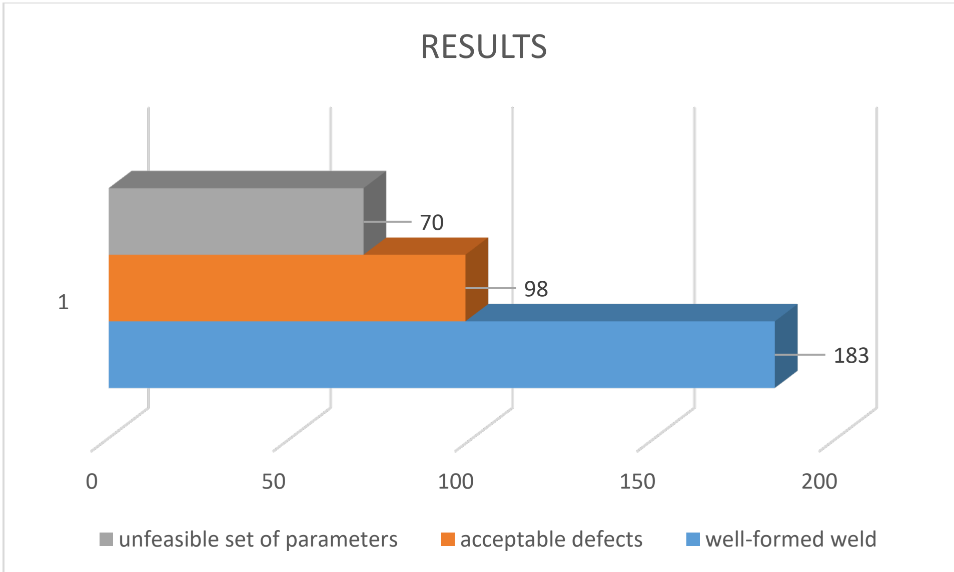

Figure 7. Results of Laser-Beam welding of Nickel-Based Alloys

Relation between Laser Power and Welding Speed

The dispersion graph obtained through MATLAB shown in Figure 8 depicts the correlation between laser power and welding speed, along with their joint influence on the quality of the weld. Below are the results of the graph obtained:

- High-quality welds (Good) are mainly found within a specific area that features moderate to high levels of laser power and intermediate welding speeds, highlighting a reliable process window.
- Conversely, poor-quality welds (Bad) tend to cluster at low laser power and low welding speeds, as well as at extreme combinations of high speeds with inadequate power, where insufficient heat input results in defects.
- Medium-quality welds (Middle) are spread across these areas, representing the transition from unstable to stable welding conditions.

In summary, the graph illustrates that weld quality is heavily influenced by the equilibrium between laser power and welding speed, underscoring the necessity of choosing suitable laser parameter combinations to attain optimal results of high-quality welding.

Figure 8. Dispersion Graph shows the relation between Laser Power (KW) and welding speed (mm/s) on weld quality.

Relation between Aluminum and Titanium on weld quality

The Al-Ti weldability map shown in Figure 9 illustrates the relationship between the Aluminum (Al) and Titanium (Ti) contents of various Ni-based superalloys and the corresponding weld quality obtained after welding. The data points are classified into three categories: good welds (green), partially defective welds (yellow), and crack welds (red). Since Al and Ti are the principal elements responsible for the formation of the strengthening γ′ precipitate phase, their concentrations strongly influence both the mechanical performance and weldability of Ni-based superalloys. In general, alloys with higher γ′ content exhibit superior high-temperature strength. However, they also become increasingly susceptible to solidification cracking and liquation cracking during welding due to reduced ductility in the partially melted zones.

A compositional relation proposed by Sekhar and Reed (Sekhar & Reed, 2002b) for conventional welding of nickel-based superalloys was considered in the present analysis. The proposed weldability criterion is expressed as:

$$2Al + Ti = 6$$

The above equation suggests adequate weldability of the alloy for values equal to or below 6**.** This relation has previously been reported in the literature as a possible compositional limit separating weldable alloys from crack-sensitive alloys. In the present weldability map, the Sekhar and Reed relation is plotted as a reference boundary to evaluate whether it can effectively distinguish between regions of good and poor weldability within the current experimental database.

However, the distribution of the data points clearly demonstrates that such a separation is not well defined for the present dataset. Crack welds (red points) are distributed on both sides of the line, while several good welds (green points) and medium welds (yellow points) are also found in regions that would theoretically be considered crack-sensitive according to the literature relation. This significant overlap indicates that the Al-Ti compositional limit proposed by Sekhar and Reed cannot reliably distinguish between weldable and non-weldable conditions for the alloys included in this study. The figure 9 further suggests that weldability behavior is more complex than a simple compositional threshold based only on Al and Ti contents. Although an overall trend can still be observed in which alloys containing lower Al and Ti concentrations generally exhibit better weldability, the presence of numerous exceptions confirms that additional metallurgical factors influence cracking susceptibility. These factors may include the total γ′ fraction, segregation behavior during solidification, grain boundary liquation, alloy chemistry beyond Al and Ti contents, welding process parameters, thermal gradients, restraint conditions, and cooling rates during solidification.

Another important feature visible in the graph is the clustering of data points in the lower-left region of the graph, corresponding to alloys with relatively low Al and Ti contents. This clustering occurs because several commercial Ni-based superalloys possess similar compositions in this compositional range. Most of these alloys exhibit good or moderate weldability, supporting the general understanding that lower γ′ forming element concentrations reduce cracking susceptibility during welding. This is indeed typical of solution-strengthened alloys, which are not strengthened by the precipitation of γ′ and are generally acknowledged to have higher weldability than precipitation alloys.

Overall, the figure demonstrates that, while the Sekhar and Reed relation provides a useful literature-based reference for conventional welding of Ni-based superalloys, it does not produce a clear weldability boundary for our database. Therefore, weldability assessment cannot rely solely on Al and Ti concentrations, and a more comprehensive approach incorporating additional metallurgical and processing variables is required to accurately predict weld cracking behavior in Ni-based superalloys.

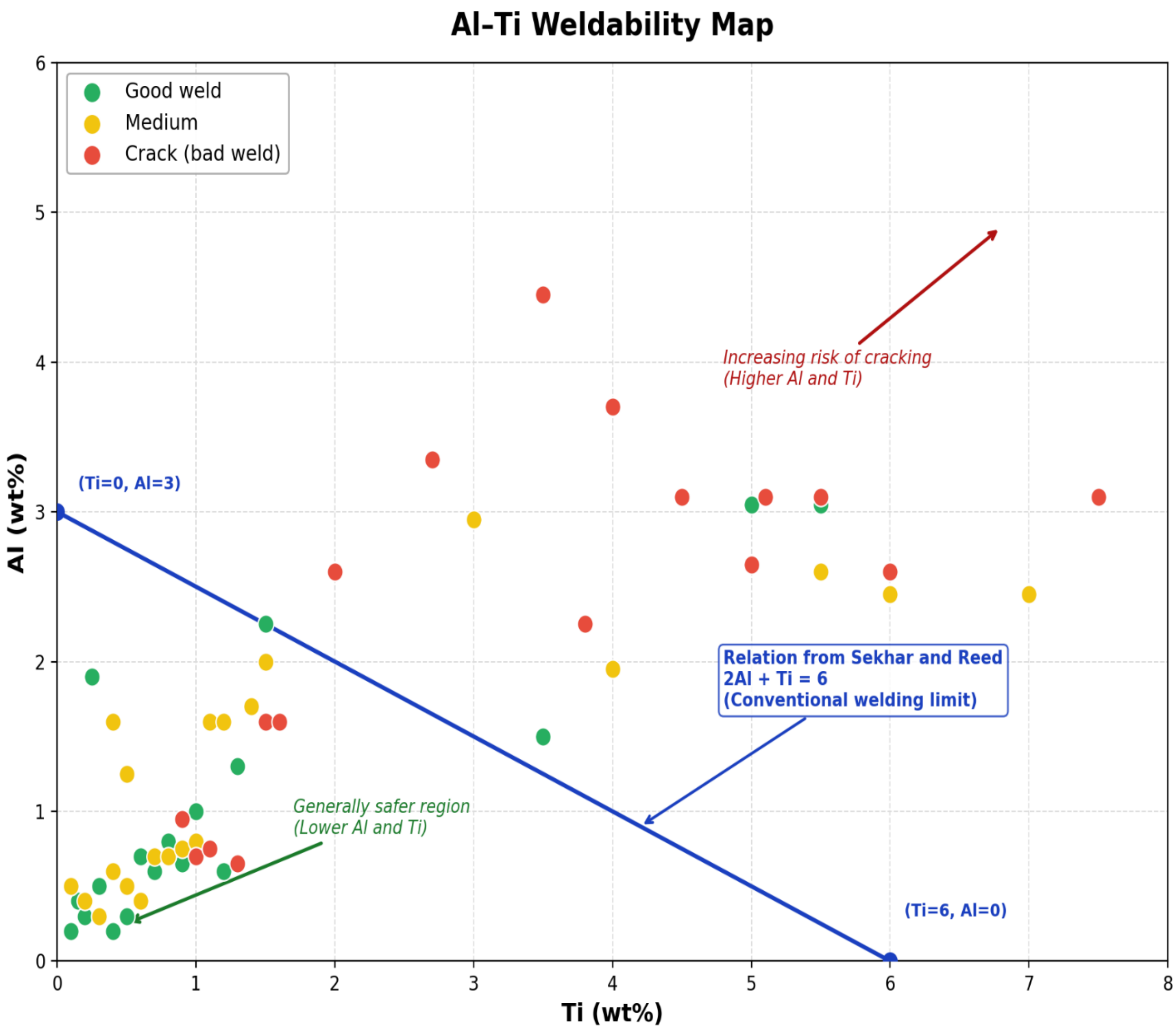

Figure 9. shows the Al-Ti compositions of different alloys and its weld quality.

Neural Network Modelling

Artificial Neural Networks (ANNs) are commonly utilized machine learning methods that can model intricate nonlinear connections between input variables and target outputs. In this research, a feedforward neural network is utilized to categorize the output classes according to the specified process and material parameters. Neural networks are well-suited for this kind of problem since conventional linear methods frequently can't account for the nonlinear interactions among process variables like material properties, laser settings, and geometric features.

The neural network model is created with MATLAB's Deep Learning Toolbox, particularly utilizing the *patternnet* function, intended for multi-class classification assignments. The input for the network was made up of the chosen predictor variables taken from the dataset, and the output matched the categorical class label specified in the OUTPUT column. The aim of the neural network is to understand the connection between the input features and the output categories and to correctly classify new, unknown samples based on the learned patterns. To guarantee appropriate training and impartial performance assessment, the dataset was split into training, validation, and testing subsets. The training set was utilized to adjust the network weights, the validation set served to oversee generalization effectiveness and avoid overfitting, and the test set was employed to assess the final performance of the trained model. The cross-entropy loss function served as the evaluation metric, as it is highly appropriate for multi-class classification issues. To guarantee consistent training and impartial evaluation, the dataset is split into three parts:

- Training set: 80%
- Validation set: 10%
- Test set: 10%

The training set is utilized to modify the network weights throughout the learning process. The validation set is employed to assess the network's performance during training and to mitigate overfitting via early stopping. The test set is exclusively reserved for the final performance assessment.

The network is trained using the cross-entropy loss function, which is frequently applied in classification tasks. Cross-entropy quantifies the difference between the predicted class probabilities and the true class labels. The training process is conducted using the built-in optimization algorithms in MATLAB, which automatically modify the network weights to reduce the cross-entropy loss.

Neural Network Implementation on MATLAB

- **Dataset import**: The data was saved in an Excel file *(.xlsx)* and brought into MATLAB with the *readtable* function. The option *VariableNamingRule = 'preserve'* was specified to maintain the original headers from Excel (including any spaces and units) without alteration. The data range was chosen so that the first row of the chosen range aligns with the header row. Once the data was loaded, any rows lacking output labels were eliminated to guarantee that all samples used for training and evaluation had valid class information.

- **Target (label):** The column OUTPUT in excel sheet, which has three class values (1, 2, and 3), was the classification goal. After extracting this column, then converting it to a numeric vector, the code determines the distinct class values. One-hot (1-of-K) encoding requires the target for neural network classification in MATLAB.

Feature (input) preparation: With the exception of the OUTPUT column, all remaining columns were used as predictors (inputs) for the neural network model. All predictor variables were numerical. Therefore, no categorical preprocessing or dummy-variable encoding was required. Before training, the input matrix was cleaned to ensure numerical stability by replacing missing and infinite values using:

X(isnan(X)) = 0;   X(isinf(X)) = 0;

This preprocessing step ensured that the neural network received only valid numerical inputs, improving training stability and preventing computational issues during cross-entropy evaluation. Following preprocessing, one feature matrix was created by linking one-hot encoded categorical features with numerical features. The final input format was set up as (features × samples), which is what MATLAB's Neural Network Toolbox functions require.

- **Data separation for testing, validation, and training:** The dataset was divided into three subgroups to guarantee an objective assessment:
  80% of the training set is utilized to update the network weights, 10% is the validation set (used for hyperparameter guiding and early terminating), 10% of the test set is used only for final performance reporting. Within MATLAB, the split was carried out automatically using:

net.divideFcn = 'dividerand', trainRatio = 0.80, valRatio = 0.10, testRatio = 0.10

- **Network architecture and training:** A classification feedforward neural network was developed using:

patternnet (size of hidden layer)

Pattern recognition (classification) is the primary purpose of patternnet. The best architecture, a single hidden layer with a 10 number of neurons was employed. As number of different architectures were applied to check the accuracy of the confusion matrix. The performance function was configured as follows:

'crossentropy' = net.performFcn

The usual loss function for multi-class classification is cross-entropy, which quantifies the discrepancy between the genuine one-hot labels and the anticipated class probabilities. The following tools were used for training:

Train(net, X, T) = [net, tr]

MATLAB tracks validation performance throughout training and automatically halts training when validation performance stops improving (early stopping). This helps to avoid the chance of overfitting.

- **Model Evaluation:** Following training, each sample's network output was calculated:

  Y = net(X)

  Then, using the index sets supplied by the training record ***tr*,** cross-entropy performance was computed independently on the training, validation, and test subsets:

  net.divideParam.trainRatio = 0.8;

  net.divideParam.valRatio = 0.1;

  net.divideParam.testRatio = 0.1;

  Lastly, plotconfusion, which offers a class-by-class breakdown of accurate predictions and misclassifications, was used to plot a confusion matrix for the test set. It is possible to assess which classes are being confused and how evenly the classification performance is distributed among the classes.

CHAPTER 4

RESULTS

The confusion and cross-entropy matrix obtained from MATLAB are shown in Figure 10 and Figure 11 respectively.

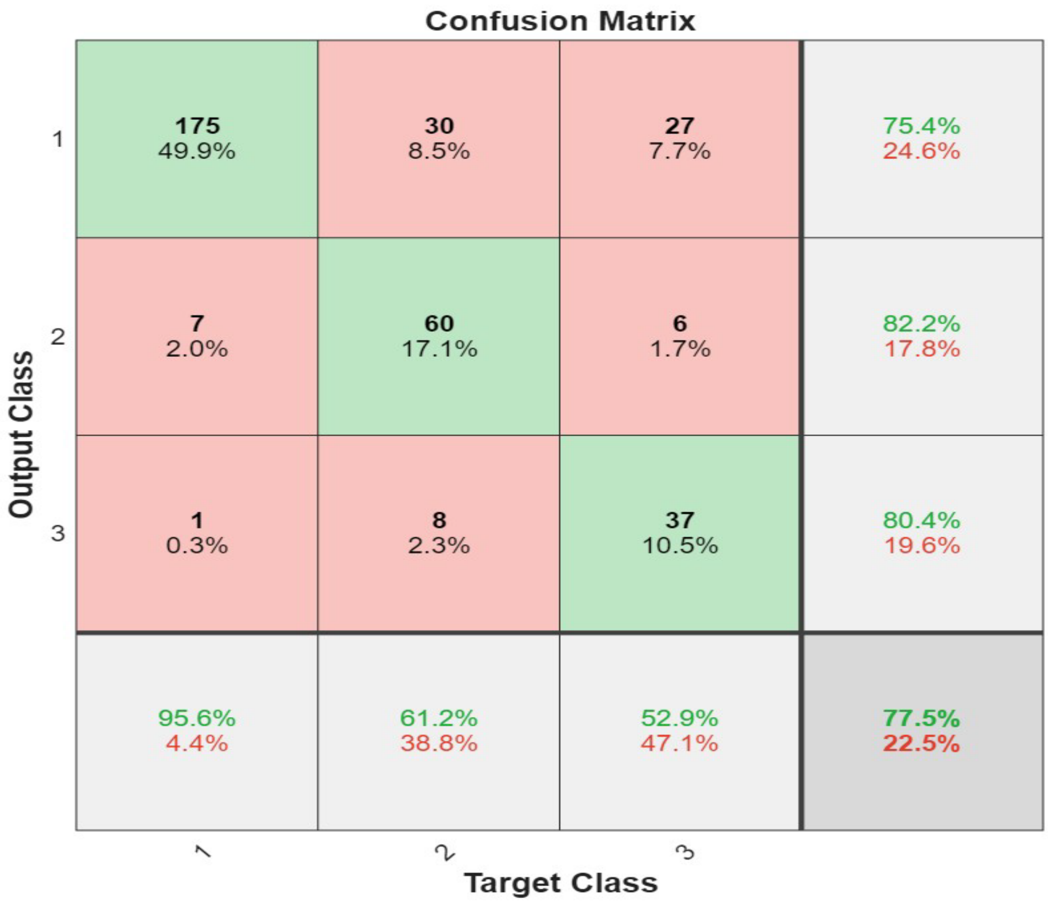

Figure 10. Confusion matrix showing classification performance of the neural network on the test dataset where Class 1 shows good Quality welds followed by Class 2 and 3 with mild and bad quality welds.

Analysis of classification performance and confusion matrix

The 3-class confusion matrix evaluates the classification performance of the developed model across three distinct classes (Class 1, Class 2, and Class 3) where Class 1 represents crack-free or safe welds, Class 2 represents moderately crack-sensitive welds, and Class 3 represents highly crack-sensitive welds. In the above confusion matrix, the columns represent the true (target) class labels, while the rows correspond to the predicted outputs of the model. The diagonal elements indicate correctly classified instances, whereas the off-diagonal elements represent misclassifications, providing insight into the model's error distribution and class-wise discriminative ability. The model demonstrates its strongest performance in Class 1, correctly identifying 175 samples, indicating a high degree of learning for this category. Class 2 and Class 3 show comparatively lower correct predictions, with 60 and 37 correctly classified instances respectively. This suggests that while the model has learned meaningful patterns across all classes, its predictive strength is significantly higher for Class 1 than for the other two classes.

The error distribution reveals notable confusion patterns between classes. For Class 1, 30 instances are misclassified as Class 2 and 27 as Class 3, indicating that Class 1 shares overlapping feature characteristics with both classes. Class 2 is relatively better separated, with only 7 instances misclassified as Class 1 and 6 as Class 3. In contrast, Class 3 shows weaker separability, with 1 instance misclassified as Class 1 and 8 as Class 2, highlighting persistent uncertainty between Class 2 and Class 3.

To evaluate the classification performance, the standard metrics of precision, recall, and accuracy are computed using the formulas below. These metrics are derived from the confusion matrix using the concepts of true positive (TP), true negative (TN), false positive (FP), and false negative (FN). A true positive represents samples correctly classified into their actual class, while a true negative represents samples correctly identified as not belonging to a given class. False positives correspond to samples incorrectly assigned to a class, whereas false negatives represent actual samples of a class that were incorrectly classified into another category.

The precision metric evaluates the reliability of positive predictions and is calculated as:

$$P = TP / (TP + FP)$$

Recall measures the ability of the model to correctly identify all actual samples of a class and is defined as:

$$R = TP / (TP + FN)$$

The overall classification accuracy indicates the proportion of correctly classified samples among the total number of samples and is calculated using:

$$\text{Accuracy} = (TP + TN) / (TP + TN + FP + FN).$$

These metrics provide a comprehensive evaluation of the model by measuring prediction correctness, class detection capability, and overall classification performance. The precision values indicate that when the model predicts a class, it is correct 75.4% of the time for Class 1, 82.2% for Class 2, and 80.4% for Class 3. However, recall values reveal a different trend, with Class 1 achieving a very high recall of 95.6%, while Class 2 and Class 3 show considerably lower recall values of 61.2% and 52.9%, respectively. This imbalance indicates that although predictions for Class 2 and Class 3 are relatively precise, the model fails to identify a substantial portion of their actual instances.

The overall classification accuracy of the model is 77.5%, with an error rate of 22.5%. While this reflects acceptable general performance, the class-wise breakdown reveals a clear bias toward Class 1, which dominates the correct predictions and recall performance.

Training results and convergence patterns

The figure below presents the evolution of cross-entropy loss for the training, validation, and test datasets over 51 epochs. Initially, all three curves exhibit a sharp decline, indicating that the model effectively learns the underlying data patterns during the early stages of training. As the epochs progress, the training loss continues to decrease steadily, while the validation loss follows a similar trend with minor fluctuations, demonstrating good generalization performance. The test loss remains consistently higher than both training and validation losses, reflecting the model's behavior on unseen data. The optimal performance is observed around epoch 45, where the validation loss reaches its minimum value, as indicated by the highlighted point and dashed lines. This epoch represents the best trade-off between bias and variance and is selected as the final model checkpoint. Beyond this point, the validation loss begins to slightly increase while the training loss continues to decrease, suggesting the onset of overfitting. Therefore, early stopping at epoch 45 ensures that the model maintains strong generalization while avoiding overfitting.

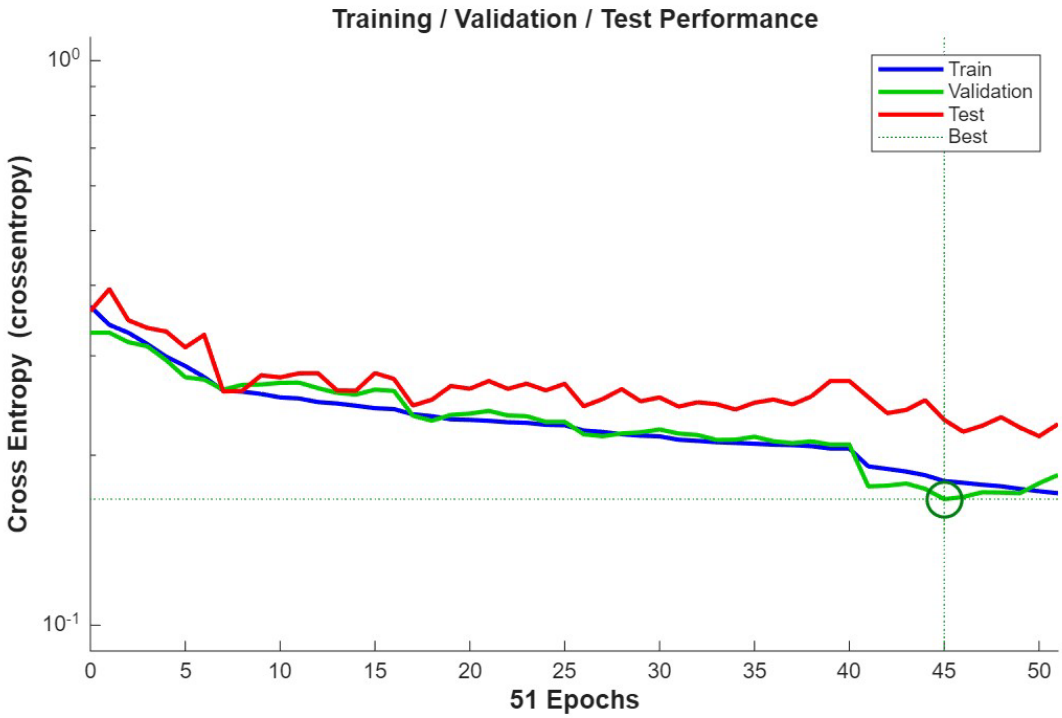

Figure 11. Cross-Entropy performance of the neural network during training

Model effectiveness and generalization capabilities

The model successfully learned the underlying relationships in the data without overfitting, as evidenced by the consistent decrease in cross-entropy during training and similar results on training, validation, and test sets. The neural network's ability to accurately predict the nonlinear relationships between the input process parameters and the output classification is demonstrated by the overall classification accuracy of 77.5% that was attained. The restricted sample size or overlapping feature distributions between specific classes are probably the causes of the few misclassifications that were noticed.

These outcomes validate the applicability of feedforward neural networks with the patternnet architecture for classification tasks requiring difficult, nonlinear manufacturing or process datasets.

Final assessment of neural network efficacy

The neural network effectively identified significant patterns from the dataset and attained consistent classification results. The findings indicate strong generalization ability, consistent training behavior, and excellent predictive performance, especially for easily recognizable classes. This verifies that neural networks are an appropriate and efficient method for tackling the classification issue.

CHAPTER 5

CONCLUSIONS

Overview of the Research

This thesis has presented a comprehensive investigation into the weldability of Nickel-based superalloys through laser beam welding (LBW), supported by a data-driven approach using Artificial Neural Networks (ANNs). The research was motivated by the critical industrial demand for high-quality, defect-free joints in nickel-based superalloys, which are indispensable materials in aerospace, power generation, and chemical processing industries. Despite their exceptional mechanical and thermal properties, these alloys pose significant challenges during welding, including susceptibility to hot cracking, liquation cracking, Laves phase formation, microstructural instability, and reduced ductility in weld zones.

To systematically address these challenges, the research was structured around two primary objectives: (1) the construction of an extensive, literature-derived database of laser beam welding experiments on various nickel-based superalloys, and (2) the development and evaluation of an Artificial Neural Network model capable of predicting weld quality based on input process parameters and alloy compositions. Together, these two pillars constitute what this thesis refers to as the Digital Weldability Test, a conceptual framework for intelligently predicting laser weld soundness without exhaustive and costly physical experimentation.

The key findings of the study are reported hereafter:

1. Key Findings from Literature Review and Database Construction

The systematic review of published literature and the resulting database, encompassing over 300 welding experiments from 73 research papers, yielded several significant insights into the laser welding behavior of nickel-based superalloys. The database covered a wide spectrum of alloys, including IN718 (Inconel 718), IN625 (Inconel 625), IN617 (Inconel 617), GTD-111, Haynes 282, Waspaloy, Rene 80, GH909, GH3535, IN800, and several newer compositions. The breadth of this dataset enabled meaningful statistical and graphical analyses of process-structure-property relationships.

The analysis of alloy distribution within the database revealed that Inconel 718 (Inconel 718) was the most extensively studied alloy, followed by Inconel 625 and GTD-111. This reflects Inconel 718's widespread industrial use, particularly in aero-engine and gas turbine applications, as well as its complex welding behavior developed from its niobium-rich composition and susceptibility to Laves phase formation. The large volume of Inconel 718 data enhanced the usefulness of the ANN model for this alloy family.

2. Effect of Laser Power and Welding Speed on Weld Quality

The dispersion graph analysis in MATLAB demonstrated that the balance between laser power and welding speed is a critical factor of weld quality. High-quality welds were predominantly observed within a well-defined process window, characterized by moderate-to-high laser power coupled with intermediate welding speeds, this ensures sufficient heat input for complete joint penetration while avoiding excessive thermal gradients that promote cracking. In contrast, poor-quality welds clustered in regions of low laser power combined with low welding speeds, as well as at extreme combinations of high speed and insufficient power, where inadequate heat input resulted in poor fusion and increased porosity. Medium-quality welds occupied transition zones between stable and unstable welding conditions. These findings confirm that an optimal process window exists for each alloy and thickness configuration, and that small deviations from this window can significantly degrade weld quality.

3. Evaluation of the Al-Ti Weldability Criterion

The Al-Ti weldability map presented in this thesis critically examined the applicability of the Sekhar and Reed compositional criterion (2Al + Ti = 6) to the current experimental dataset. While this criterion has been widely cited in literature as a boundary separating weldable from crack-sensitive nickel-based superalloys in conventional welding, the analysis revealed that it does not provide a reliable division for laser beam welded alloys in this database.

Cracked welds (red points) were found on both sides of the boundary line, while acceptable and good-quality welds were also present in regions theoretically classified as crack-sensitive. Although an overarching trend was observed, alloys with lower Al and Ti concentrations generally exhibited better weldability and the extensive data scatter and overlap between quality classes confirmed that Al and Ti content alone is insufficient to predict weld cracking susceptibility. Other influential variables, such as process parameters, thermal gradients, restraint conditions, and cooling rates, also play critical roles in determining weldability. This finding underscores the necessity of a multi-variable predictive approach, which the ANN model addresses effectively.

4. Performance of the Artificial Neural Network Model

The ANN model, developed using MATLAB's Deep Learning Toolbox with the patternnet architecture, was trained on the compiled database to classify weld outcomes into three categories: good welds (Class 1), welds with acceptable defects (Class 2), and defective or cracked welds (Class 3). The model incorporated process parameters (laser power, welding speed, material thickness) and alloy composition variables (Ni, Al, Ti, Cr, Fe) as inputs, with one-hot encoding applied to categorical alloy identifiers.

5. Classification Accuracy and Confusion Matrix Analysis

The neural network achieved an overall classification accuracy of 77.5% on the test dataset, demonstrating its ability to capture the complex, nonlinear relationships between input parameters and weld quality. The confusion matrix revealed that the model performed most strongly for Class 1 (good welds), correctly identifying 175 out of the test samples for this class, with a recall of 95.6%. This high recall reflects the model's effective learning of the conditions associated with sound weld formation, which is of greatest practical importance in welding quality assurance.

Class 2 achieved a precision of 82.2% but a relatively lower recall of 61.2%, while Class 3 showed a precision of 80.4% and the lowest recall of 52.9%. The weaker performance for Classes 2 and 3 is attributable to several factors: (i) fewer training samples for these categories due to the imbalanced nature of the dataset, (ii) overlapping feature distributions between classes, as many process conditions produce results near the boundary between acceptable and defective welds, and (iii) the inherently stochastic nature of weld defect formation, which is influenced by material inhomogeneities and microstructural variability not fully captured by the input features.

6. Training Convergence and Generalization Behavior

The cross-entropy loss evolution curves showed consistent and well-behaved convergence across training, validation, and test subsets over 51 epochs. All three loss curves exhibited a sharp initial decline, indicative of rapid and effective learning in the early stages of training. The optimal model checkpoint was identified at epoch 45, where the validation loss reached its minimum. Beyond this epoch, slight upward divergence between training and validation losses indicated the early onset of overfitting, which was effectively mitigated by the early stopping mechanism implemented in MATLAB. This convergence behavior reflects that the chosen architecture, a single hidden layer with 10 neurons, provided sufficient model capacity to represent the data while avoiding excessive parameter redundancy.

The consistent proximity of the test loss to the validation loss throughout training further confirms that the model generalized well to unseen data and was not overfitted to the training set. This is a particularly important result given the relatively modest size of the dataset, and it validates the appropriateness of the 80-10-10 data split strategy and the regularization provided by the cross-entropy performance function.

Contributions of the Research

This research makes several significant contributions to the field of welding science, materials engineering, and intelligent manufacturing:

- The database compiled in this thesis constitutes one of the most extensive publicly referenced datasets on laser beam welding of nickel-based superalloys, covering over 300 experimental entries from 73 papers and spanning more than 20 distinct alloy systems. This database serves as a valuable resource for future machine learning and metallurgical studies.
- The application and testing of the Sekhar-Reed Al-Ti weldability criterion against a large, diverse LBW dataset revealed its limitations for laser welding applications, contributing to a deeper understanding of the conditions under which conventional weldability models fail.
- The ANN model developed in this thesis demonstrates that machine learning can effectively predict laser weld quality from process parameters and alloy composition, achieving 77.5% overall accuracy. This represents a meaningful step toward intelligent, data-driven welding process design.
- By combining process data with machine learning, this thesis lays the conceptual and technical groundwork for a Digital Weldability Test, a virtual tool capable of predicting weld soundness from input parameters alone, reducing the need for costly trial-and-error experimentation in advanced manufacturing.

Limitations of the Study

Although the results of this study are encouraging, there are some important limitations that should be kept in mind:

- The dataset used to train the model contained over 300 experiments, which is a reasonable starting point but still relatively small for a neural network. More importantly, most of the data belonged to Class 1 (good welds), while Classes 2 and 3 (mild and defective welds) had far fewer entries. This imbalance made it harder for the model to correctly identify poor-quality welds.

- The model only used inputs that were commonly reported across most studies, such as laser power, welding speed, material thickness, and basic alloy composition. Many other factors that can affect weld quality, like beam focus size, shielding gas, surface preparation, and heat treatment were not consistently available in the literature and could not be included.
- The weld quality ratings (good, acceptable, or bad) were taken directly from the judgments of different research teams around the world. Since different researchers may assess weld quality slightly differently, there is a chance of some inconsistency in the labels used to train the model.

Recommendations for Future Work

Building upon the findings and limitations identified in this thesis, the following recommendations are proposed for future research:

- Future work should focus on expanding the database with additional experimental data, particularly for under-represented alloy systems and defective weld categories. Standardized data collection protocols across research groups would significantly improve label consistency and data quality.
- The predictive power of the model could be significantly enhanced by including additional metallurgical and process variables such as the total gamma-prime fraction, heat input (as a derived parameter), pulse characteristics, beam focus offset, and post-weld heat treatment conditions.
- Exploration of more sophisticated architectures such as convolutional neural networks (CNNs) for image-based weld quality assessment, ensemble methods, or hybrid physics-informed neural networks could yield improved predictive accuracy and interpretability.

- The model's predictions should be validated against newly conducted, independent welding experiments, particularly for alloy-parameter combinations not represented in the current database, to assess its generalizability in real manufacturing environments.
- Future iterations of the Digital Weldability Test could be integrated with optimization algorithms (e.g., genetic algorithms etc.) to automatically identify optimal parameter windows for new alloy compositions, covering the way for autonomous welding process design.

Final Remarks

This thesis demonstrates that the integration of laser beam welding expertise with artificial intelligence methodologies offers a powerful and promising approach to the long-standing challenge of predicting weld quality in Nickel-based superalloys. The ANN model developed in this work successfully captured the complex, nonlinear dependencies between alloy composition, process parameters, and weld quality outcomes, achieving 77.5% classification accuracy across three weld quality categories.

The Digital Weldability Test concept put forward in this research represents a significant step toward intelligent, data-driven manufacturing. In industries where the cost of weld failure can be catastrophic, from aero-engine turbine blades to nuclear reactor components, a reliable computational tool for pre-screening parameter combinations before physical trials can deliver substantial benefits in terms of time, cost, and material efficiency.

Although the present model has limitations rooted in dataset size, class imbalance, and feature scope, it establishes a solid methodological foundation upon which more powerful and comprehensive future models can be built. With continued development, the Digital Weldability Test has the potential to become an indispensable tool in the welding engineer's toolkit, enabling faster alloy qualification, reduced experimentation costs, and higher confidence in the structural integrity of laser-welded nickel-based superalloy components across the most demanding engineering applications.

REFERENCES

Aghayar, Y., Naghashzadeh, A. R., & Atapour, M. (2021a). An assessment of microstructure and mechanical properties of inconel 601/ 304 stainless steel dissimilar weld. *Vacuum*, *184*. https://doi.org/10.1016/j.vacuum.2020.109970

Aghayar, Y., Naghashzadeh, A. R., & Atapour, M. (2021b). An assessment of microstructure and mechanical properties of inconel 601/ 304 stainless steel dissimilar weld. *Vacuum*, *184*. https://doi.org/10.1016/j.vacuum.2020.109970

Ahmad, G. N., Raza, M. S., Singh, N. K., & Muvvala, G. (2021a). Investigating the effect of process parameters on weld pool thermal history and mechanical properties of laser welded Inconel 625 and Duplex stainless steel 2205 dissimilar welds. *Optik*, *248*. https://doi.org/10.1016/j.ijleo.2021.168134

Ahmad, G. N., Raza, M. S., Singh, N. K., & Muvvala, G. (2021b). Investigating the effect of process parameters on weld pool thermal history and mechanical properties of laser welded Inconel 625 and Duplex stainless steel 2205 dissimilar welds. *Optik*, *248*. https://doi.org/10.1016/j.ijleo.2021.168134

Aina, J. O. (2014). *A STUDY OF LASER WELDABILITY OF IN-738 NICKEL-BASED SUPERALLOY IN A NEW PRE-WELD HEAT TREATMENT CONDITION*.

Akca, E., & Gürsel, A. (2015). A Review on Superalloys and IN718 Nickel-Based INCONEL Superalloy. *Periodicals of Engineering and Natural Sciences (PEN)*, *3*(1). https://doi.org/10.21533/pen.v3i1.43

Allen, C., Shaw-Edwards, R., & Nijdam, T. (2015). Nickel-containing superalloy laser weld qualities and properties. *Journal of Laser Applications*, *27*(S2). https://doi.org/10.2351/1.4906301

Alswat, H. M. (2025). Influence of laser power on mechanical and microstructural behavior of Nd: YAG laser welding of Incoloy alloy 800. *High Temperature Materials and Processes*, *44*(1). https://doi.org/10.1515/htmp-2025-0084

Alvarez, P., Vázquez, L., Ruiz, N., Rodríguez, P., Magaña, A., Niklas, A., & Santos, F. (2019). Comparison of hot cracking susceptibility of tig and laser beam welded alloy 718 by varestraint testing. *Metals*, *9*(9). https://doi.org/10.3390/met9090985

Ariaseta, A., Pick, D., Andersson, J., & Ojo, O. (2024). Study of Pulsed Laser Beam Welding of Nickel-Based Superalloy G27. *Advances in Transdisciplinary Engineering*, *52*, 39–49. https://doi.org/10.3233/ATDE240152

Arulmurugan, B., Kumar, M. S., Kannan, T., Karuppiah, S., Kumaraguru, N., Ponsundar, E., Ragu, G., & Manikandan, M. (2021). Investigation on mechanical and microstructure characteristics of nickel based c-2000 super alloy using laser beam welding. *Materials Today: Proceedings*, *43*, 3044–3049. https://doi.org/10.1016/j.matpr.2021.01.393

Caiazzo, F., Alfieri, V., Cardaropoli, F., & Sergi, V. (2017). Investigation on edge joints of Inconel 625 sheets processed with laser welding. *Optics and Laser Technology*, *93*, 180–186. https://doi.org/10.1016/j.optlastec.2017.03.011

Cburnett. (2006). *An example artificial neural network with a hidden layer*.

Chen, Z., & Taheri, M. (2020). The effect of pre-heating and pre-cold treatment on the formation of liquation and solidification cracks of nickel-based superalloy welded by laser beam. *Journal of Materials Research and Technology*, *9*(5), 11162–11177. https://doi.org/10.1016/j.jmrt.2020.07.053

Cheng, B., Huang, X., Zhang, M., Mao, C., Wu, D., Zhou, D., Ma, G., Tang, K., & Luo, B. (2024). Microstructure and properties of laser welding Ni-based alloy/austenitic stainless steel with filler wire for nuclear reactor pump can end sealing. *Journal of Materials Research and Technology*, *30*, 1929–1938. https://doi.org/10.1016/j.jmrt.2024.03.239

Cheng, H. L. K. (2022). *Dynamic behavior of molten pool backside during full-penetration laser welding of Ni-based superalloys*.

Devendranath Ramkumar, K., Pavan, B., & Chandrasekar, V. (2018). Development of improved microstructural traits and mechanical integrity of stabilized stainless steel joints of AISI 321. *Journal of Manufacturing Processes*, *32*, 582–594. https://doi.org/10.1016/j.jmapro.2018.03.029

Donnini, R., Varone, A., Palombi, A., Spiller, S., Ferro, P., & Angella, G. (2025). High Energy Density Welding of Ni-Based Superalloys: An Overview. In *Metals* (Vol. 15, Number 1). Multidisciplinary Digital Publishing Institute (MDPI). https://doi.org/10.3390/met15010030

E.O. Ezugwu, Z.M. Wang, & A.R. Machado. (1999). The machinability of nickel-based alloys: a review. *ELSEVIER*.

García-Sesma, L., Álvarez, P., Gorostegui-Colinas, E., Huarte, I., & Santos, F. (2024). Alternatives to Reduce Hot Cracking Susceptibility of IN718 Casting Alloy Laser Beam Welds with a Mushroom Shape. *Metals*, *14*(9). https://doi.org/10.3390/met14091067

Ghaffari, R., & Naffakh-Moosavy, H. (2022). Investigation of macrostructure, microstructure, and hot cracking susceptibility of laser-welded Inconel-718 superalloy under various post-cold treatment environments. *CIRP Journal of Manufacturing Science and Technology*, *37*, 110–124. https://doi.org/10.1016/j.cirpj.2022.01.007

Gobbp, S., Zhang, L., Norris, J., Richteff, K. H., & Loreau, J. H. (1996). Materials Processing Technology HIGH POWDER CO2 AND Nd-YAG LASER WELDING OF WROUGHT INCONEL 718. In *Journal of Materials Processing Technology* (Vol. 56).

Graneix, J., Beguin, J. D., Pardheillan, F., Alexis, J., & Masri, T. (2014). Weldability of the superalloys Haynes 188 and Hastelloy X by Nd:YAG. *MATEC Web of Conferences*, *14*. https://doi.org/10.1051/matecconf/20141413006

Graneix, J., Béguin, J.-D., Alexis, J., Masri, T., Ré Mie Graneix, J., Beguin, J., & Alexis, L. (2017). Influence of Yb:YAG laser beam parameters on Haynes 188 weld fusion zone microstructure and mechanical properties Influence of Yb:YAG laser beam parameters on Haynes 188 weld fusion zone microstructure and mechanical properties Open Archive Toulouse Archive Ouverte (OATAO) Influence of Yb:YAG Laser Beam Parameters on Haynes 188 Weld Fusion Zone Microstructure and Mechanical Properties. *Metallurgical and Materials Transactions B*, *48*(n°4), 2007–2016. https://doi.org/10.1007/s11663-017-0989-6ï

Hamada, A., Ghosh, S., Rautio, T., Jaskari, M., Abd-Elaziem, W., & Järvenpää, A. (2025). Strengthening and embrittlement mechanisms in laser-welded additively manufactured Inconel 718 superalloy. *Welding in the World*, *69*(1), 81–98. https://doi.org/10.1007/s40194-024-01897-0

Hong, J. K., Park, J. H., Park, N. K., Eom, I. S., Kim, M. B., & Kang, C. Y. (2008). Microstructures and mechanical properties of Inconel 718 welds by CO2 laser welding. *Journal of Materials Processing Technology*, *201*(1–3), 515–520. https://doi.org/10.1016/j.jmatprotec.2007.11.224

Hong, M., Wang, S., Sun, W., Geng, Z., Xin, J., & Ke, L. (2022). Effect of welding speed on microstructure and mechanical properties of selective laser melting Inconel 625 alloy laser welded joint. *Journal of Materials Research and Technology*, *19*, 2093–2103. https://doi.org/10.1016/j.jmrt.2022.06.020

Hou. Wang.Yong. (2023). *Effect of Temperatures on Mechanical Properties and Microstructure Evolution of Laser-Welded Ni-Base Superalloy*.

Hu, X. A., Xue, Z. Y., Zhao, G. Le, Yun, J., Shi, D., & Yang, X. G. (2019). Laser welding of a selective laser melted Ni-base superalloy: Microstructure and high temperature mechanical property. *Materials Science and Engineering: A*, *745*, 335–345. https://doi.org/10.1016/j.msea.2018.12.081

Huang, X., Zhang, H., Wang, Z., Li, J., Geng, Y., Zhou, X., Li, X., & Bai, Z. (2025). Comparative study on the weldability and mechanical performance of IN718, ATI 718Plus alloy in laser beam welding. *Materials Science and Engineering: A*, *929*. https://doi.org/10.1016/j.msea.2025.148133

Iskindar Tili. (2022). *Numerical and experimental analysis of temperature distribution and melt flow in fiber laser welding of Inconel 625*.

Janaki Ram, G. D., Venugopal Reddy, A., Prasad Rao, K., Reddy, G. M., & Sarin Sundar, J. K. (2005). Microstructure and tensile properties of Inconel 718 pulsed Nd-YAG laser welds. *Journal of Materials Processing Technology*, *167*(1), 73–82. https://doi.org/10.1016/j.jmatprotec.2004.09.081

Jaya Kishore Sunkara. (2024). *Experimental Investigation of the Metallurgical and Mechanical Properties of an Nd: YAG Laser-Welded Inconel-825 Superalloy*.

Jelokhani-Niaraki, M. R., B. Mostafa Arab, N., Naffakh-Moosavy, H., & Ghoreishi, M. (2016). The systematic parameter optimization in the Nd:YAG laser beam welding of Inconel 625. *International Journal of Advanced Manufacturing Technology*, *84*(9–12), 2537–2546. https://doi.org/10.1007/s00170-015-7833-4

Jiang, Z., Tao, W., Yu, K., Tan, C., Chen, Y., Li, L., & Li, Z. (2016). Comparative study on fiber laser welding of GH3535 superalloy in continuous and pulsed waves. *Materials and Design*, *110*, 728–739. https://doi.org/10.1016/j.matdes.2016.08.055

Keivanloo, A., Naffakh-Moosavy, H., & Miresmaeili, R. (2021). The effect of pulsed laser welding on hot cracking susceptible region size and weld pool internal geometry of Inconel 718: Numerical and experimental approaches. *CIRP Journal of Manufacturing Science and Technology*, *35*, 787–794. https://doi.org/10.1016/j.cirpj.2021.09.001

Khan, M. M. A., Romoli, L., Fiaschi, M., Dini, G., & Sarri, F. (2012). Laser beam welding of dissimilar stainless steels in a fillet joint configuration. *Journal of Materials Processing Technology*, *212*(4), 856–867. https://doi.org/10.1016/j.jmatprotec.2011.11.011

Kumar, A., Chauhan, V., & Singh Bist, A. G. (2013). Role of Artificial Neural Network in Welding Technology: A Survey. In *International Journal of Computer Applications* (Vol. 67, Number 1).

Lee, H. T., Jeng, S. L., & Kuo, T. Y. (2003). *The Microstructure and Fracture Behavior of the Dissimilar Alloy 690-SUS 304L Joint with Various Nb Addition* (Vol. 34).

Li . M Gao . Chen. (2013). *Characterisation comparison of laser and laser–arc hybrid welding of Invar 36 alloy*.

LI, Z., ZHANG, Z. lin, WU, A. ping, ZHANG, M. jun, KANG, J., LIU, Q., ZHAO, Y., & CHEN, J. yang. (2024). Microstructure and mechanical properties of laser welded and post-weld heat-treated K439B superalloy. *Transactions of Nonferrous Metals Society of China (English Edition)*, *34*(3), 905–917. https://doi.org/10.1016/S1003-6326(23)66442-8

Lijun Yang. (2024). *Complete-joint-penetration vacuum laser beam welding of nickel-based superalloy 718Plus*.

Liu, B. X., Yin, F. X., Dai, X. L., He, J. N., Fang, W., Chen, C. X., & Dong, Y. C. (2017). The tensile behaviors and fracture characteristics of stainless steel clad plates with different interfacial status. *Materials Science and Engineering: A*, *679*, 172–182. https://doi.org/10.1016/j.msea.2016.10.033

Ma, G., Wu, D., Niu, F., & Zou, H. (2015). Microstructure evolution and mechanical property of pulsed laser welded Ni-based superalloy. *Optics and Lasers in Engineering*, *72*, 39–46. https://doi.org/10.1016/j.optlaseng.2015.03.009

Montazeri, M., & Ghaini, F. M. (2012). The liquation cracking behavior of IN738LC superalloy during low power Nd:YAG pulsed laser welding. *Materials Characterization*, *67*, 65–73. https://doi.org/10.1016/j.matchar.2012.02.019

Moradi, M., & Ghoreishi, M. (2011). Influences of laser welding parameters on the geometric profile of NI-base superalloy Rene 80 weld-bead. *International Journal of Advanced Manufacturing Technology*, *55*(1–4), 205–215. https://doi.org/10.1007/s00170-010-3036-1

Murua, O., Arrizubieta, J. I., Lamikiz, A., & Schneider, H. I. (2024). A Case Study of a Laser Beam Welding Model for the Welding of Inconel 718 Sheets of a Dissimilar Thickness. *Metals*, *14*(7). https://doi.org/10.3390/met14070829

Naffakh Moosavy, H., Aboutalebi, M. R., Seyedein, S. H., Goodarzi, M., Khodabakhshi, M., Mapelli, C., & Barella, S. (2014). Modern fiber laser beam welding of the newly-designed precipitation- strengthened nickel-base superalloys. *Optics and Laser Technology*, *57*, 12–20. https://doi.org/10.1016/j.optlastec.2013.09.030

Norouzian, M., Amne Elahi, M., & Plapper, P. (2023). A review: Suppression of the solidification cracks in the laser welding process by controlling the grain structure and chemical compositions. In *Journal of Advanced Joining Processes* (Vol. 7). Elsevier B.V. https://doi.org/10.1016/j.jajp.2023.100139

OdabaşI, A., Ünlü, N., Göller, G., & Eruslu, M. N. (2010). A study on laser beam welding (LBW) technique: Effect of heat input on the microstructural evolution of superalloy inconel 718. *Metallurgical and Materials Transactions A: Physical Metallurgy and Materials Science*, *41*(9), 2357–2365. https://doi.org/10.1007/s11661-010-0319-y

Odabaşi, A., Ünlü, N., Göller, G., Kayali, E. S., & Eruslu, M. N. (2013). Assessment of the effects of heat input on microstructure and mechanical properties in laser beam welded Haynes 188 undermatched joints. *Materials Science and Engineering: A*, *559*, 731–741. https://doi.org/10.1016/j.msea.2012.09.017

Osoba, L. O., Ding, R. G., & Ojo, O. A. (2012). Microstructural analysis of laser weld fusion zone in Haynes 282 superalloy. *Materials Characterization*, *65*, 93–99. https://doi.org/10.1016/j.matchar.2011.12.009

Osobo . Oja. (2011). *Influence of laser welding heat input on HAZ cracking in newly developed Haynes 282 superalloy*.

Pakniat, M., Ghaini, F. M., & Torkamany, M. J. (2016). Hot cracking in laser welding of Hastelloy X with pulsed Nd: YAG and continuous wave fiber lasers. *Materials and Design*, *106*, 177–183. https://doi.org/10.1016/j.matdes.2016.05.124

Palanivel, R., Dinaharan, I., Laubscher, R. F., & Alarifi, I. M. (2021). Effect of Nd:YAG laser welding on microstructure and mechanical properties of Incoloy alloy 800. *Optics and Laser Technology*, *140*. https://doi.org/10.1016/j.optlastec.2021.107039

Pang, M., Yu, G., Wang, H. H., & Zheng, C. Y. (2008). Microstructure study of laser welding cast nickel-based superalloy K418. *Journal of Materials Processing Technology*, *207*(1–3), 271–275. https://doi.org/10.1016/j.jmatprotec.2007.12.091

Pariyar, A., John, A., Perugu, C. S., Edachery, V., & Kailas, S. V. (2023). Influence of laser beam welding parameters on the microstructure and mechanical behavior of Inconel X750 superalloy. *Manufacturing Letters*, *35*, 33–38. https://doi.org/10.1016/j.mfglet.2022.11.005

Patil, S. A., Jha, A., Ganesh, P. S., Petley, V. U., Rajeswari, S., Shariff, S. M., Ramji, M., & Muvvala, G. (2025). A study on laser welding of Inconel 718 and evolution of strain field using digital image correlation to estimate the localized properties. *Optics and Laser Technology*, *184*. https://doi.org/10.1016/j.optlastec.2025.112472

Prakash, L., Kumar, C., Gogai, D., Kumar, M., & Devi, S. (2024). Laser Beam Welding of Inconel Alloys: A Review. *Journal of Physics: Conference Series*, *2818*(1). https://doi.org/10.1088/1742-6596/2818/1/012047

Qian, M., & Lippold, J. C. (n.d.). *Liquation Phenomena in the Simulated Heat-Affected Zone of Alloy 718 after Multiple Postweld Heat Treatment Cycles Delta-phase formation increases fiquation cracking susceptibility*.

Ren, W., Lu, F., Yang, R., Liu, X., Li, Z., & Elmi Hosseini, S. R. (2015). A comparative study on fiber laser and CO2 laser welding of Inconel 617. *Materials and Design*, *76*, 207–214. https://doi.org/10.1016/j.matdes.2015.03.033

Rogl, P. F., & Chen, X. (2013). Intermetallics, Interstitial Compounds and Metallic Glasses in High-Entropy Alloys. *Science Direct*.

Roy, A., Pamarthi, V. V., Kumar, N., & Masters, I. (2025). Analysis of Stirring Action to Control Grain Refinement of Inconel 625 Superalloy Bead on Plate Using Laser Wobble Technology. *Journal of Materials Engineering and Performance*, *34*(8), 6916–6925. https://doi.org/10.1007/s11665-024-10625-0

Saurabh, S. K., Chand, P., & Yadav, U. S. (2024). Multi-objective optimization and fracture analysis of laser weld joints of Ni-Cr superalloy 80 A for gas turbine components. *Journal of Mechanical Science and Technology*, *38*(9), 4867–4876. https://doi.org/10.1007/s12206-024-0822-5

Seenivasan. (2025). *Metallurgical and Mechanical Characterization of Optimized Ytterbium Fiber Laser-Welded Inconel 718 Similar Joints*.

Sekhar, N. C., & Reed, R. C. (2002a). Power beam welding of thick section nickel base superalloys. *Science and Technology of Welding and Joining*, *7*(2), 77–87. https://doi.org/10.1179/136217102225002628

Sekhar, N. C., & Reed, R. C. (2002b). Power beam welding of thick section nickel base superalloys. *Science and Technology of Welding and Joining*, *7*(2), 77–87. https://doi.org/10.1179/136217102225002628

Shanthos Kumar. (2018). *Numerical and experimental studies on the effect of varied pulse energy in Nd:YAG laser welding of Monel 400 sheets*.

Sharma, S. K., Biswas, K., Nath, A. K., Manna, I., & Dutta Majumdar, J. (2020). Microstructural change during laser welding of Inconel 718. *Optik*, *218*. https://doi.org/10.1016/j.ijleo.2020.165029

Shoja Razavi, R. (2016). Laser beam welding of Waspaloy: Characterization and corrosion behavior evaluation. *Optics and Laser Technology*, *82*, 113–120. https://doi.org/10.1016/j.optlastec.2016.03.011

Sorell, G. (1997). *CORROSION-AND-HEAT-RESISTANT NICKEL ALLOYS: GUIDELINES FOR SELECTION AND APPLICATION*.

Taheri, M., Halvaee, A., & Kashani-Bozorg, S. F. (2019). Effect of Nd:YAG pulsed-laser welding parameters on microstructure and mechanical properties of GTD-111 superalloy joint. *Materials Research Express*, *6*(7). https://doi.org/10.1088/2053-1591/ab1534

Taheri, M., Kazemi, A., Gurusamy, P., Rasoulpouraghdam, A., Mohanavel, V., Ravichandran, M., & Paidar, M. (2022). Features of hybrid laser-arc welding of GTD-111 superalloy compared to laser beam welding. *Materials Letters*, *309*. https://doi.org/10.1016/j.matlet.2021.131384

Taheri, M., Razavi, M., Kashani-Bozorg, S. F., & Torkamany, M. J. (2021). Relationship between solidification and liquation cracks in the joining of GTD-111 nickel-based superalloy by Nd:YAG pulsed-laser welding. *Journal of Materials Research and Technology*, *15*, 5635–5649. https://doi.org/10.1016/j.jmrt.2021.11.007

Thejasree, P., Binoj, J. S., Manikandan, N., Krishnamachary, P. C., Raju, R., & Palanisamy, D. (2020). Multi objective optimization of wire electrical discharge machining on Inconel 718 using Taguchi grey relational analysis. *Materials Today: Proceedings*, *39*, 230–235. https://doi.org/10.1016/j.matpr.2020.06.517

Thejasree, P., Manikandan, N., Binoj, J. S., Varaprasad, K. C., Palanisamy, D., & Raju, R. (2020). Numerical simulation and experimental investigation on laser beam welding of Inconel 625. *Materials Today: Proceedings*, *39*, 268–273. https://doi.org/10.1016/j.matpr.2020.07.042

Thejasree, P., Manikandan, N., Raju, R., Narasimhamu, K. L., Surendranatha, G. M., & Damodaram, A. K. (2022a). Investigations on laser beam welded Inconel 718 weldments. *Materials Today: Proceedings*, *68*, 1757–1761. https://doi.org/10.1016/j.matpr.2022.09.442

Thejasree, P., Manikandan, N., Raju, R., Narasimhamu, K. L., Surendranatha, G. M., & Damodaram, A. K. (2022b). Investigations on laser beam welded Inconel 718 weldments. *Materials Today: Proceedings*, *68*, 1757–1761. https://doi.org/10.1016/j.matpr.2022.09.442

Tian, Z., Chen, S., Wang, Y., Tao, W., Ye, X., Li, N., Ren, W., & Yang, S. (2023). Laser welding of GH3539 alloy for molten salt reactor: Processing optimization, microstructure and mechanical properties. *Materials Characterization*, *205*. https://doi.org/10.1016/j.matchar.2023.113266

Tian, Z., Chen, S., Wang, Y., Tao, W., Ye, X., Ren, W., & Yang, S. (2023). Dynamic laser welding hot cracking behavior and mechanism of new structural material Ni–28W–6Cr alloy for molten salt reactor. *Journal of Materials Research and Technology*, *25*, 3022–3036. https://doi.org/10.1016/j.jmrt.2023.06.170

Tian, Z., Chen, S., Wang, Y., Ye, X., Tao, W., & Yang, S. (2024). Study on the mechanism of Ni-26W-6Cr alloy solidification cracking: Effect of laser welding heat input. *Materials Letters*, *357*. https://doi.org/10.1016/j.matlet.2023.135779

Vemanaboina, H., Gundabattini, E., Akella, S., Uma Maheshwar Rao, A. C., Buddu, R. K., Ferro, P., & Berto, F. (2021a). Mechanical and metallurgical properties of co2 laser beam inconel 625 welded joints. *Applied Sciences (Switzerland)*, *11*(15). https://doi.org/10.3390/app11157002

Vemanaboina, H., Gundabattini, E., Akella, S., Uma Maheshwar Rao, A. C., Buddu, R. K., Ferro, P., & Berto, F. (2021b). Mechanical and metallurgical properties of co2 laser beam inconel 625 welded joints. *Applied Sciences (Switzerland)*, *11*(15). https://doi.org/10.3390/app11157002

Voropaev, A., Stramko, M., Sorokin, A., Logachev, I., Kuznetsov, M., & Gook, S. (2019). Laser welding of Inconel 718 nickel-based alloy layer-by-layer products. *Materials Today: Proceedings*, *30*, 473–477. https://doi.org/10.1016/j.matpr.2019.12.399

Yan, F., Hu, C., Zhang, X., Cai, Y., Wang, C., Wang, J., & Hu, X. (2017). Influence of heat input on HAZ liquation cracking in laser welded GH909 alloy. *Optics and Laser Technology*, *92*, 44–51. https://doi.org/10.1016/j.optlastec.2017.01.016

Yan, S., Meng, Z., Chen, B., Tan, C., Song, X., & Wang, G. (2022). Experimental study on the grain evolution induced by thermal characteristics during oscillation laser welding of IN718. *Materials Letters*, *323*. https://doi.org/10.1016/j.matlet.2022.132581

Yang . Huiping . Zhou. (2025). *Numerical Simulation and Experimental Analysis of Laser Welding of GH4099 Ni-Based Superalloy Thin Plate*.

Yeni. Kocak. (2006). *Fracture toughness analysis of laser-beam-welded superalloys Inconel 718 and 625*.

Yilbas, B. S., & Akthar, S. (2011). Laser welding of Haynes 188 alloy sheet: Thermal stress analysis. *International Journal of Advanced Manufacturing Technology*, *56*(1–4), 115–124. https://doi.org/10.1007/s00170-011-3181-1

Yoshiki Oshida, & Toshihiko Tominaga. (2020). Nickel Titanium Material. *De Gruyter Bill*.

Yu, K., Jiang, Z., Li, C., Chen, S., Tao, W., Zhou, X., & Li, Z. (2017). Microstructure and Mechanical Properties of Fiber Laser Welded GH3535 Superalloy. *Journal of Materials Science and Technology*, *33*(11), 1289–1299. https://doi.org/10.1016/j.jmst.2016.11.026

Yue, N., Pei, L., Xu, P., Jiang, Z., Lin, T., Zhou, L., & Liang, Y. (2024). Porosity suppression of nickel-based superalloy by modulated base temperature in laser welding and mechanism analysis. *Journal of Materials Research and Technology*, *30*, 4725–4738. https://doi.org/10.1016/j.jmrt.2024.04.199

Yuguang, Z., Kai, X., & Dongyan, S. (2013). An improved artificial neural network for laser welding parameter selection and prediction. *International Journal of Advanced Manufacturing Technology*, *68*(1–4), 755–762. https://doi.org/10.1007/s00170-013-4796-1

Zapirain, F., Zubiri, F., Garciandía, F., Tolosa, I., Chueca, S., & Goiria, A. (2011). Development of laser welding of Ni based superalloys for aeronautic engine applications (experimental process and obtained properties). *Physics Procedia*, *12*(PART 1), 105–112. https://doi.org/10.1016/j.phpro.2011.03.014

Zhang . Yang. (2022). *Microstructural Characteristics of Laser Welded Joints of GH909 ...2*.

Zhang, X., Zhu, Z., Ma, X., Wang, C., Mi, G., & Zheng, S. (2021). Solidification features and tensile performance altered by increased welding speed during laser welding GH909 superalloy. *Materials Characterization*, *181*. https://doi.org/10.1016/j.matchar.2021.111488

Zhengwu Zhu. (2022). *Optimization of beam oscillation on macro/micro formation and mechanical property in low-expansion superalloy laser-welded joint*.

Zhu, Z., Ma, X., Mi, G., & Wang, C. (2020). Electron microscopy study of laser welded GH909 superalloy joint. *Journal of Materials Research and Technology*, *9*(6), 15525–15536. https://doi.org/10.1016/j.jmrt.2020.10.049